Simulations of Eddy currents in the Seville spherical tokamak

Daniel López Aires

email: danlopair@alum.us.es

Supervisors: Carlos Soria del Hoyo[1] and Eleonora Viezzer[2]

Faculty of Physics, University of Seville

June 25, 2019

[1]Department of Electronics and Electromagnetism, Faculty of Physics, University of Seville

[2]Department of Atomic, Molecular and Nuclear Physics, Faculty of Physics, University of Seville

Abstract

Achieving controlled nuclear fusion on Earth could be a decisive aspect on the climate change fight. It is also an exciting field because of its scientific and technological challenges. The Plasma Science and Fusion Technology group of the University of Seville is planning to build a magnetic fusion device, a *spherical tokamak* for research in different aspects on controlled nuclear fusion. This bachelor thesis is the first numerical study on the vessel and coils configuration of the future Seville Spherical Tokamak. It analyzes four different configurations taking into accout both plasma equilibria and dynamical aspects plasma discharge.

The fundamentals of toroidal magnetic fusion devices such as spherical tokamaks are explained. An study study of four different configurations for the Seville spherical tokamak is carried out using the FIESTA code. The main parameters of the four configurations are compared, providing the best shape of the spherical tokamak, as well as valuable information about the coilset configuration of the device.

Acknowledgements

I would like to thank my advisors, Eleonora, for giving me the chance to work on this project, and Carlos, without whom this work would not have been possible. Thanks to Manolo, who has been the "unofficial third advisor" of this work, for all his advices. I would also like to thank Alessio, who has just started his PhD with the Plasma Science and Fusion Technology Group, for his help.

Agradecer a mi familia por su apoyo, y sobre todo su comprensión, y a mis amigos, tanto estepeños, que no os olvido aunque no nos veamos últimamente, como a los amigos de la facultad, por todos los buenos momentos pasados durante estos cuatro duros años, así como todas las bolas disfrutadas. Gracias.

Contents

Chapter 1

Introduction

1.1 Nuclear fusion as an energy source

Nowadays, the human kind is beginning to understand the damage its activity is causing on Earth, that could lead to the destruction of the planet we live in and, as a consequence, of ourselves. A radical change is needed in human's life before it is too late. One fundamental step is to cease using fossil fuels as an energy source, and use renewable sources instead, like wind energy, solar energy, or geothermal energy. However, there is another energy source, virtually renewable[1] that could provide a huge step forward this transition, *nuclear fusion*.

Nuclear fusion is a type of nuclear reaction in which two or more light atomic nuclei (reactants) interact and produce a heavier nuclei and other subatomic particles (neutrons and protons), releasing or absorbing a certain amount of energy, determined by the difference of mass of the elements involved.

The Sun and all the stars emit energy due to nuclear fusion. In the stars, the reactants are confined due to gravitational forces. Can nuclear fusion be used as an energy source? Is its possible to create a Sun on Earth? Human beings certainly can not create an object ass massive as a star on Earth, but a device to obtain energy from, making use of a certain fusion reaction could be created. This is called *controlled nuclear fusion*. To use controlled nuclear fusion as an energy source on Earth, the most desirable reaction due

[1] Virtually means that it is enough fuel for thousands of years on Earth. This will be explained later.

to its cross-section is[2]

$$ {}^{2}_{1}\mathrm{D} + {}^{3}_{1}\mathrm{T} \rightarrow {}^{4}_{2}\mathrm{He} + {}^{1}_{0}n + 17.6\mathrm{MeV}, \tag{1.1} $$

where the total kinetic energy released is $17.6MeV$, and ${}^{2}_{1}\mathrm{D}$ and ${}^{3}_{1}\mathrm{T}$ are deuterium and tritium respectively, two isotopes of hydrogen[3]. To stimulate this reaction, the reactants have to be heated up to ~ 10 keV (is is usual to name $k_B T$ as temperature, where k_B is the Boltzmann constant), that is, about 100 millions celsius degree, to overcome the Coulomb repulsion between nuclei. This is called *thermonuclear fusion*. At this temperature, the fuel (deuterium and tritium) is in the plasma state. *A plasma is a quasineutral gas of charged and neutral particles which exhibits collective behavior*[5].

To use nuclear fusion as an energy resource, it is mandatory that the power obtained P_{fus} exceed the power applied to the system P_{app}. The Q factor is usually introduced, which is the ratio between the power obtained and the power applied to the system,

$$ Q = \frac{P_{\text{fus}}}{P_{\text{app}}}, \tag{1.2} $$

so $Q > 1$ is needed.

The thermonuclear power per unit volume is the product of the reaction rate per unit volume $\mathcal{R}$ and the energy released per reaction E_{rel}, which is, if we total ion density if n, and the densities of deuterium and tritum are $n/2$[6]

$$ P = \mathcal{R} E_{\text{rel}} = \frac{1}{4} n^2 < \sigma v > E_{\text{rel}}, \tag{1.3} $$

where $< \sigma v >$ is the averaged value of the product of the relative velocity of the particles and the cross-section of the reaction. However, there exists energy losses in the magnetic confinement approach, leading to a loss power P_{l}, which can be expressed as, if W is the plasma energy

[2] That is, this reaction that has the greatest cross-section for the lowest energy of the reactants,as can be seen in [1], section 1.2 .

[3] Deuterium can be extracted form the sea, and tritium can be obtained by a fission reaction of lithium, which is an abundant element on Earth. This is why it is said that nuclear fusion is virutally renewable, because there is enough fuel for thousands of years, without creating long-live radioacive waste[4]

[5] This is the definition given in [2].

[6] See [1], section 1.3 .

$$P_{\mathrm{l}} = \frac{W}{\tau_{\mathrm{e}}}, \tag{1.4}$$

where τ_{e} is called the *energy confinement time*. That is, the plasma tend to lose energy cooling itself down, so plasma heating is needed, providing an applied power P_{app}.

The D-T reaction produced an α particle ($^4_2$He nuclei) carrying 3.5MeV and a neutron carrying 14.1MeV. The neutron, since it is neutral, leave the plasma without interacttion but the α particles are confined by the magnetic field, and it can transfer its energy to the plasma by collision with the plasma particles. This is called α-*heating*. The power balance requires that the power applied to the plasma plus the heating power have to balance the loss power, $P_{\mathrm{app}} + P_\alpha = P_{\mathrm{l}}$.

The α-particles heating suggest a scenario in which there would not be neccesary to apply external heating could be achieved. This would mean $Q \to \infty$. This is called *ignition*, and the condition to achieve it is the *Lawson criterion*,[7]

$$nT\tau_{\mathrm{e}} > 5 \cdot 10^{21} \mathrm{m}^{-3} \mathrm{keV\ s}. \tag{1.5}$$

The Lawson criterion can be satisfied with magnetic confinement, which means the plasma must be maintained during a time τ_{e} with a density n and a temperature T.

1.2 Definition of a plasma

The definition of a plasma of [2] has been previously said, *a plasma is a quasineutral gas of charged and neutral particles which exhibits collective behavior*. The definitions of collective behaviour and quasineutrality are as follow:

- *Quasineutrality*. A plasma is composed of neutral and charged particles, ions and electrons, such that the net charge is zero. A neutral plasma (in equilibrium) will have the same charged particle density, n_0. Assuming for both ions and electrons the same charge, e, if a point charge q is inserted in the plasma, the electrostatic potential is, if the coordinate system is centered at the test charge

$$\phi(r) = \frac{1}{4\pi\epsilon_0}\frac{q}{r}\exp\left[\frac{-r}{\lambda_{\mathrm{Debye}}}\right] \equiv \phi_0(r)\exp\left[\frac{-r}{\lambda_{\mathrm{Debye}}}\right], \tag{1.6}$$

[7] See [1], section 1.5 .

where $\phi_0(r)$ is the vacuum potential the point charge, and $\lambda_{\text{Debye}} = \sqrt{\frac{\epsilon_0 k_B T_e}{e^2 n_0}}$ is the Debye length, with T_e the plasma temperature. This means that the potential is shielded if $r > \lambda_{Debye}$. Therefore, if the size of the plasma L is much greater than λ_{Debye}, any charge accumulation will be shielded, so that the plasma remains neutral. $L >> \lambda_{\text{Debye}}$ is the *quasineutrality condition*.

However, the shielding of local charge accumulations could only be done if the plasma has enough particles surrounding the charge accumulation to shield it, and this leads to another condition, $N_D >> 1$, where $N_D = n_0 \frac{4}{3}\pi\lambda_{Debye}^3$ is the number of particles in a sphere of radius λ_{Debye} surrrounding the charge, called the "Debye sphere". This two conditions have to be satisfied to achieve quasineutrality.

- *Collective behaviour*. This means that the motion of the gas has to be governed mainly by electromagnetic forces rather than hydrodynamic forces, i.e. collisions between the particles. If ω is the frequency of typical plasma oscillations and τ is the mean time between collisions with neutral atoms, the condition for an ionized gas to behave like a plasma is $\omega\tau > 1$.

An ionized gas is considered a plasma if the three previous condition are satisfied (the two conditions of quasineutrality and the condition of collective behaviour).

1.3 Motion of a charged particle in a magnetic field

If a particle of charge q is set in a magnetic field $\vec{B}$, the field exerts a force upon the charged particle given by Lorentz's law:

$$\vec{F}_{\text{mag}} = q\vec{v} \wedge \vec{B}, \tag{1.7}$$

where $\vec{v}$ it the velocity of the particle. Note that the force is perpendicular to the velocity; if q moves an amount $d\vec{l} = \vec{v}dt$, the work done by the magnetic force is $dW = \vec{F}_{\text{mag}} \cdot d\vec{l} = q\vec{v} \wedge \vec{B} \cdot \vec{v}dt = 0$. The Lorentz force, hence, can not speed up the particle, but it can modify the trajectory of the particle.

To explore the motion of the particle, the simpler case is the case of a constant magnetic field $\vec{B}_0$. The equation of motion in an inertial frame is, by Newtons's second law

$$m\frac{d\vec{v}}{dt} = \vec{F}_{\text{mag}} = q\vec{v} \wedge \vec{B}_0, \tag{1.8}$$

where m is the mass of the particle. If we assume $\vec{B}_0 = B_0 \hat{z}$, (1.8) leads to

$$\left.\begin{aligned} m\frac{dv_x}{dt} &= qB_0 v_y, \\ m\frac{dv_y}{dt} &= -qB_0 v_x, \\ m\frac{dv_z}{dt} &= 0, \end{aligned}\right\} \Rightarrow \left.\begin{aligned} \frac{d^2v_x}{dt^2} &= -\omega_c^2 v_x, \\ \frac{d^2v_y}{dt^2} &= -\omega_c^2 v_y, \\ m\frac{dv_z}{dt} &= 0, \end{aligned}\right\} \tag{1.9}$$

where $\omega_c \equiv qB_0/m$ is the *Larmor frequency*. The solution of (1.9) can be written as

$$\left.\begin{aligned} v_x(t) &= v_\perp \cos(\omega_c t), \\ v_y(t) &= v_\perp \sin(\omega_c t), \\ v_z(t) &= v_\parallel, \end{aligned}\right\} \Rightarrow \left.\begin{aligned} x(t) &= x(0) + R_{\text{L}} \sin(\omega_c t), \\ y(t) &= y(0) - R_{\text{L}} \cos(\omega_c t), \\ z(t) &= z(0) + v_\parallel t, \end{aligned}\right\} \tag{1.10}$$

where $v_\perp$ and $v_\parallel$ are the modules of the component of the velocity perpendicular and paralell to the magnetic field respectively, $(x(0), y(0), z(0))$ is the initial position of the particle and $R_{\text{L}} \equiv v_\perp/\omega_c$ is the *Larmor radius*. The particle describes a circular motion of radius R_{L} in the plane perpendicular to the field, centered on $(x(0), y(0))$, and an uniform motion paralell to the field, due to its velocity along the magnetic field, that is, if follows an helical motion. The axis of this helix is called *guiding centre*. Figure 1.1 shows this motion.

For more complex situations, like the presence of an electric field or non-uniform electromagnetic fields, one approach to understand the total motion of the particle is to treat separately the additional force that acts upon the particle, which results either on an acceleration parallel to the magnetic field or a drift of the guiding centre. The most common are going to be briefly mentioned:

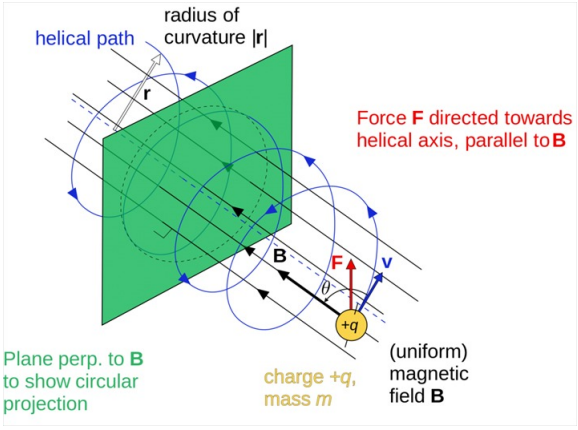

Figure 1.1. Motion of a charged particle in an uniform magnetic field. The particle follows an helical trajectory. Source: google images, 2019.

- Acceleration due to $E_\parallel$

  A parallel (to the magnetic field) electric field $E_\parallel$ provides an acceleration given by

$$m\frac{dv_\parallel}{dt} = qE_\parallel \tag{1.11}$$

- Acceleration due to $(\nabla B)_\parallel$, magnetic mirror effect

  If the magnetic field has a gradient parallel to $\vec{B}$ (B is the magnitude of the magnetic field, so ∇B is a vector), and the particle has a velocity perpendicular to $\vec{B}$, there is a force parallel to the magnetic field, which can be used to confine the particle. It is easier to understand by considering energy conservation, and treating the charged particle as a magnetic dipole of magnetic moment $\mu = mv_\perp^2/2B$ The force upon the particles is then

$$\vec{F} = -\mu(\nabla B)_\parallel \frac{\vec{B}}{B} \tag{1.12}$$

  where $(\nabla B)_\parallel$ is the parallel component of (∇B).

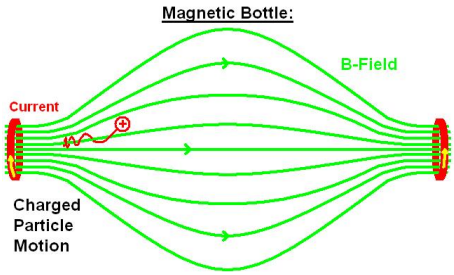

Figure 1.2. Magnetic bottle. The conservation of the energy and the magnetic moments enables the confinement of particles with this set up. Source: google images, 2019.

It can be shown[8] that μ is an adiabatic invariant, which means it remains almost constant during the motion of the particle. Consider a non-uniform magnetic field displaying regions of low and high magnetic field intensity, like the one on figure 1.2, called *magnetic bottle*. The conservation of the energy and the magnetic moment in two points i and f leads to

$$\begin{aligned} E_\mathrm{i} = E_\mathrm{f} \Rightarrow \frac{1}{2}m(v_{i\perp}^2 + v_{i\parallel}^2) = \frac{1}{2}m(v_{f\perp}^2 + v_{f\parallel}^2), \\ \mu_\mathrm{i} = \mu_\mathrm{f} \Rightarrow \frac{mv_{\mathrm{i}\perp}}{2B_\mathrm{i}} = \frac{mv_{\mathrm{f}\perp}}{2B_\mathrm{f}}. \end{aligned} \tag{1.13}$$

[8] See [1], section 2.7 .

If the field B increases from point i to f, $v_\perp$ has to increase too, which means that $v_\parallel$ has to decrease. This suggests that if the field is large enough, a point f with $v_{f\parallel} = 0$ can exist, and in this point the particle bounces (by the action of the force) and moves in the opposite direction.

- $\vec{E} \wedge \vec{B}$ drift

  The drift velocity of the guiding centre $\vec{v_d}$ due to a force $\vec{F}$ is

$$\vec{v}_d = \frac{1}{q}\frac{\vec{F} \wedge \vec{B}}{B^2}. \tag{1.14}$$

  With an electric field perpendicular to the magnetic field, the particle undergoes the so-called $\vec{E} \wedge \vec{B}$ drift, which can be easily computed by using (1.14) with $\vec{F} = q\vec{E}$, resulting in a motion independent on the charge. This motion is shown in figure 1.3 (a).

- ∇B drift

  If we have a ∇B perpendicular to $\vec{B}$, the Larmor radius will vary and a result, the total motion of the particle will be an egg-shaped motion (see figure 1.3 (b)). The drift velocity is given by

$$\vec{v}_{\nabla B} = \frac{mv_\perp^2}{2q}\frac{\vec{B} \wedge \nabla B}{B^3}. \tag{1.15}$$

- Curvature drift

  If the guiding centre of a charged particle is following a curved field line, it undergoes a drift due to the centrifugal force. If the field lines have a constant radius of curvature R_c, the drift velocity is

$$\vec{v}_c = \frac{mv_\parallel^2}{qB^2}\frac{\vec{R}_c \wedge \vec{B}}{B^2}, \tag{1.16}$$

  where $\vec{R}_c$ points from the center of the radius of curvature towards the outside (See fig 1.3 (c)).

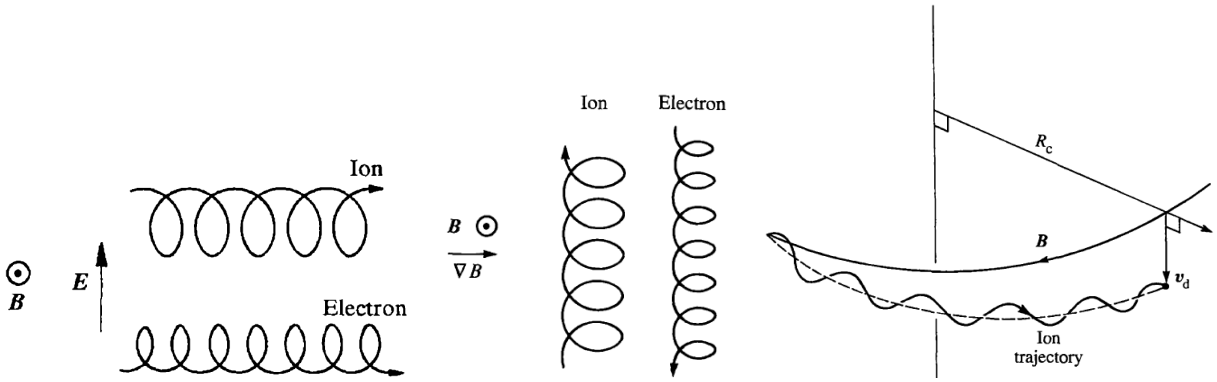

(a) $\vec{E} \wedge \vec{B}$ drift on ion and electron. The drift velocity points to the right, so both ions and electrons move to the right, since this drift do not depend on the charge, modifying the circular motion into an egg-shaped motion.

(b) ∇B drift on ion and electron. The drift velocity points upward or downward, depending on the charge.

(c) Curvature drift of an ion due to a curved magnetic field. It is shown the direction of the drift velocity.

Figure 1.3. $\vec{E} \wedge \vec{B}$, ∇B and curvature drifts. Source: [1].

1.4 Magnetic fusion devices

Many devices have been created to pursue nuclear fusion by magnetic confinement. The basis of one of the first devices, magnetic mirrors, have been described. Here we are going to focus on toroidal devices. The devices currently under research to achieve nuclear fusion through magnetic confinement are based on toroidal geometries. If a toroidal solenoid is considered, it is a closed geometry with a magnetic field that is null at its outside and it goes as $1/R$ at its inside, according to Ampère's law, where R is the radial coordinate (see figure 2.1 (a)). However, this is not enough to confine particles inside the solenoid because of the drifts described previously. The non-uniformity of the magnetic field at its inside leads to a ∇B drift, that drift the ions downward and the electrons upward, since (1.15) depends on the charge q. This charge separation will create an electric field perpendicular to the magnetic field, so the particles will experience a $\vec{E} \wedge \vec{B}$ drift, that would drift outward both ions and electrons, provided that this drift does not depend on the charge. These drifts are shown in figure 1.4 (a). Two devices that overcomes this drifts are stellarators and tokamaks.

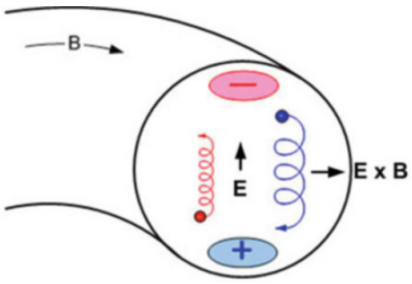

(a) Drifts in a torus. Source: [2].

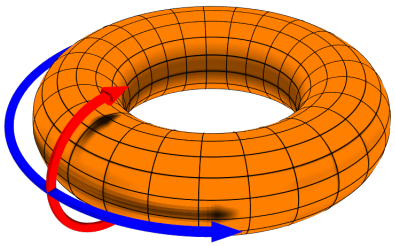

(b) Toroidal (blue) and poloidal (red) directions of a torus. Source: google images, 2019.

Figure 1.4. Drifts in a torus and definition of the poloidal and toroidal directions on a torus.

1.4.1 Stellarators

One way to solve the drifts discussed above is to twist the torus creating an 8-shaped torus. By doing this, it can be overcomed the $\vec{E} \wedge \vec{B}$ drift because in one half this drift will push the particles outward, but in the other half will push them inward. This is device is called *stellarator*. This name refers to the fact that stars use fusion power as an energy resource, and this device was designed to do it too. However, an easier way to cancel this drift was discovered later, and it was to add a helical set of coils around the torus, so that the plasma is twisted, and the magnetic field lines (superposition of the toroidal magnetic field[9] created by the coils of the torus and the helical coils) are wound hellicaly along the plasma. Particles then are mostly confined.

For the stellarator start-up, both a suitable magnetic field, and initial plasma heating is needed. The plasma heating can be made by serveral ways, like ohmic heating (a current in the plasma is induced, that will heat the plasma according to the Joule's heating law, $P_{\text{diss}} = I^2 \cdot R$), electromagnetic waves (the electromagnetic waves will create oscillations of the plasma particles, increasing their energy), injection of neutral particles (the particles throught collisions with the plasma plasma particles will speed them up, increasing their temperature), and many more[10]. One of the advantages of stellarators with respect to

[9] The toroidal and poloidal directions of a torus are showed in figure 1.4 (a). The magnetic field of the coilset of the torus then goes in the toroidal direction, so it is usually called toroidal magnetic field.

[10] See chapter 5 of [1] for a description of heating methods, that could be applied both to tokamaks and stellarators. It can be learned more about the heating methods of stellarators by searching currently

tokamaks is that stellarators can work continuisly, while a tokamak is, nowadays, made for opperate in pulsed regime.

Figures 1.5 shows an sketch of an stellarator, displaying the toroidal magnetic field coils, the helical field coils, the vessel (grey-coloured), the resulting helical plasma (purple), and the twisted magnetic field lines (green arrows).

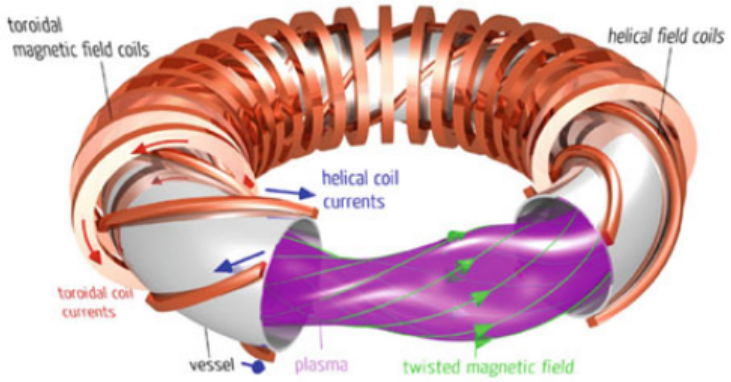

Figure 1.5. Sketch of an stellarator with helical coils, displaying its elements. Source: [2].

1.4.2 Tokamaks

Tokamaks rely on the same principle to confine particles, the creation of twisted magnetic field lines. However, in tokamaks the poloidal magnetic field (magnetic field in the poloidal direction) that adds to the toroidal magnetic field is created by the plasma itself [11]. Its name is a Russian acronym for toroidal chamber with an axial magnetic field. Tokamaks display toroidal symmetry, a feature stellarators usually do not have. Tokamaks need a set of poloidal magnetic field (PF) coils for shape control of the plasma, that is: to maintain the plasma within the vessel, overcoming the forces that pushes the plasma outward (see the begining of section 1.4), and to overcome instabilities. The interaction between the PF coils and the plasma can be understood by considering the interaction between two conductors, since the plasma can be regarded as a large conductor provided that it carries an electrical current. The interaction of two wires is showed in figure 1.6.

Figure 1.7 shows a sketch of a tokamak with its basics elements. The plasma in contained in the vacuum vessel (grey coloured in the figure). The toroidal field (green

oppperating stellarators, like Wendelstein 7-X (https://www.ipp.mpg.de/w7x).

[11] See [1] for a rigurous treatment of Tokamaks. For a more divulgative, yet formal and descriptive point of view, it is highly recommended to see [3, 4, 5, 6]

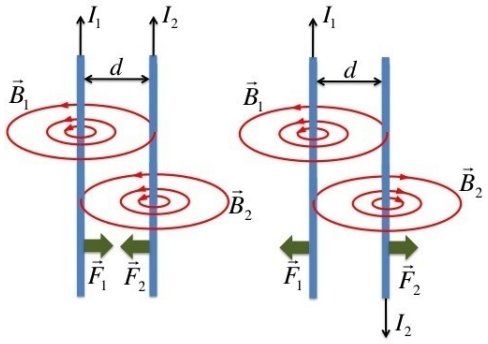

Figure 1.6. Magnetic forces between two wires carrying currents in the same and opposite directions, showing also the magnetic field of the wires. The Force in wire 1 due to the wire 2 is $F_{1,2} = \int I_1 \vec{dl} \wedge \vec{B_2}$, where $\vec{dl}$ is a differential element of the wire 1, with the same direction as the current, I_1, and the integral extends to all the length of the wire 1. The interaction between the PF coils and the plasma is similar, since the plasma can be regarded as a huge wire ($I\vec{dl}$ would be substitued by $\vec{j}dV$ in the case of volume current). Source: google images, 2019 .

arrows) is created by the toroidal magnetic field coils, and the poloidal field is created mainly by the plasma itself, and by the PF coils. In the center of the device there is a transformer coil that induces a toroidal current in the plasma (red arrows) that creates the poloidal magnetic field. The resulting field lines are helical lines (yellow arrows), which confine most of the particles of the plasma. Since the plasma current is inductive, Tokamaks operate in a pulsed regime. For a tokamak start-up, a suitable toroidal magnetic field and plasma heating is needed, and also an inductor to induce a current of the plasma is needed. This inductor will start the so-called *tokamak discharges*. One of the disadvantages of tokamaks is the presence of disruptions, which are events that end up the discharge that are based in the loss of the plasma thermal energy due to instabilities, which are not well understood. Stellarators do not suffer these events.

Which one is the most suitable device to use in an hypothethical nuclear fusion power plant? There is no clear answer to that question nowadays, since both have physical and technical advantages and drawbacks [12]. For instance, stellarators may have more technological difficulties due to its complex shape, but in the other hand tokamaks operates in pulsed regimes which ends abruptly due to disruptions. The ITER experiment (International Thermonuclear experimental reactor) will study the hypothetical use of a tokamak in a power plant[13].

[12]For an advanced comparison, see [7].

[13]See the ITER webpage, https://www.iter.org/, for more details about the ITER project.

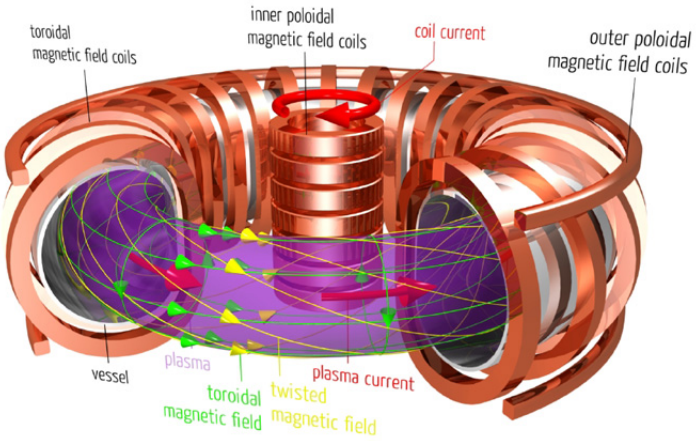

Figure 1.7. Sketch of a tokamak, showing its basic elements, the field lines and the plasma current. Source: google images, 2019.

This thesis will be centered on tokamaks. It is usual to classify tokamaks according to its aspect ratios (see figure 1.8 (a) for the definition of aspect ratio). When the aspect ratio of the tokamak is < 2, the device is called *spherical tokamak* (See figure 1.8 (b)).

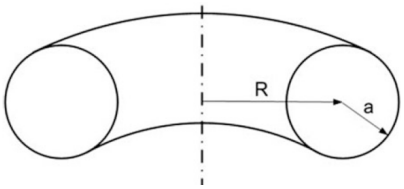

(a) A circular torus with aspect ratio R/a. Source: [2].

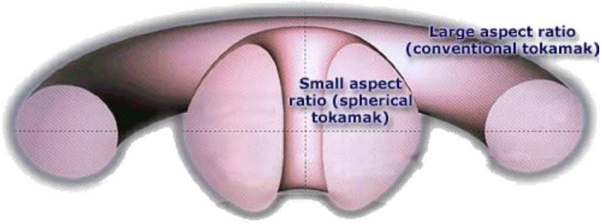

(b) Tokamaks and spherical tokamaks. Source: Manuel García Muñoz, Plasma Science and Fusion Technology group.

Figure 1.8. Definition of aspect ratio and comparison between tokamaks and spherical tokamaks.

Nowadays, spherical tokamaks are the most desirable approach to achieve controlled nuclear fusion on Earth, and the main reasons are[14]

- Small size, which implies smaller costs
- Fusion power. spherical tokamaks's plasmas displays a natural elongation which provides higher thermonuclear power than regular tokamaks (at the end of section 2.3.2 it is given the formula that explains this).

[14]See [8] for a detailed explanation of spherical torus plasmas.

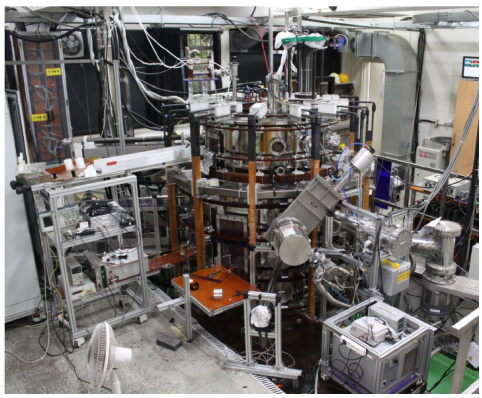

(a) VEST tokamak, in Korea. Photograph given by Y.S. Hwang and VEST team.

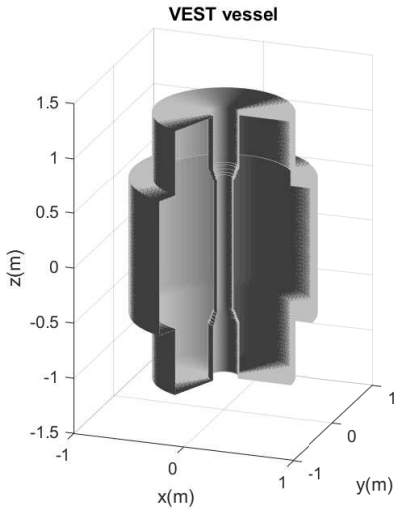

(b) Vessel of the VEST tokamak, made with the FIESTA code.

Figure 1.9. VEST tokamak, in Korea

The Plasma Science and Fusion Tecnology group of the University of Seville is planning to build an spherical tokamak (ST) in Centro Nacional de aceleradores (CNA), in Seville. The Versatile Experiment spherical torus (VEST), located in Korea, showed in figure 1.9 has been taken as a reference to design the Seville ST.

The goal of this thesis it to start the search for the best tokamak scenario; looking for the most stable equilibrium of the plasma, the currents required to achieve that equilibrium, as well as their position, and to calculate the eddy currents in the vacuum vessel. The eddy current distribution in the vessel is a key aspect in the design process, since it provides information about the temperature of the vessel (by the Joule's heating law), as well of the magnetic forces the vessel has to withstand. It also provides information about the real magnetic field inside the vessel, since the eddy currents will also create field inside the vessel.

Chapter 2

Theoretical Background

In this chapter the fundamental concepts needed to understand this thesis are described.

2.1 Magnetohydrodynamic model of a plasma

The Magnetohydrodynamic (MHD) model is a single fluid description of a plasma, i.e., it is a model that treats a plasma like a continuum matter, rather than as a set of particles. This is one of the easier models to study a plasma, and it assumes several hypothesis, like quasineutrality or negligible electron inertia[1].

The set of equations are

$$\frac{\partial \rho}{\partial t} + \nabla \cdot (\rho \vec{v}) = 0, \text{ [Mass conservation]} \tag{2.1}$$

$$\rho\Big[\frac{\partial \vec{v}}{\partial t} + (\vec{v} \cdot \nabla)\vec{v}\Big] = \vec{j} \wedge \vec{B} - \nabla p, \text{ [Momentum conservation]} \tag{2.2}$$

$$\vec{E} + \vec{v} \wedge \vec{B} = \eta \vec{j}, \text{ [Ohm's law]} \tag{2.3}$$

$$\frac{\partial}{\partial t}(p\rho^{-\gamma}) + (\vec{v} \cdot \nabla)(p\rho^{-\gamma}) = 0, \text{ [Adiabatic behaviour]} \tag{2.4}$$

$$\nabla \wedge \vec{E} = -\frac{\partial \vec{B}}{\partial t}, \tag{2.5}$$

$$\nabla \wedge \vec{B} = \mu_0 \vec{j}, \tag{2.6}$$

$$\nabla \cdot \vec{B} = 0, \tag{2.7}$$

where ρ is the plasma density, $\vec{v}$ its velocity, η its resistivity, p its pressure (in general the pressure is a tensor, but for this simplified model, it is considered an scalar magnitude),

[1] See any book about plasma physics for further details, like [2].

$\vec{j}$ its current density, γ is the adiabatic index, and $\vec{E}$ and $\vec{B}$ the electric and magnetic field the generated by the plasma. Note that the last three equations are a quasi-static limit of the Maxwell's equations.

2.2 Grad-Shafranov equation

Figure 2.1(a) displays the coordinate system of toroidal devices. In an equilibrium situation, the magnetic field of a Tokamak produces an infinite set of nested toroidal magnetic flux surfaces[2] as shown in figure 2.2, and the magnetic field lines follow an helical path on them as they wind round the torus. The poloidal flux Ψ and the toroidal flux Φ between two magnetic surfaces are defined by

$$d\Psi \equiv \vec{B} \cdot d\vec{S}_{\mathrm{p}}, \quad d\Phi \equiv \vec{B} \cdot d\vec{S}_{\phi}, \tag{2.8}$$

where dS_{p}, $dS_{\phi} \equiv dS_{\mathrm{T}}$ are the poloidal and toroidal surface elements, whose magnitude are defined in Figure 2.1(b) (its unitary vector is perpendicular to the surface, and the sign is arbitrary, as usually in the magnetic fluxes), and $\vec{B}$ is the magnetic field. The basic condition for the equilibrium is that the force on the plasma be zero at all points, so the momentum conservation equation (2.2) leads to[3]

$$\vec{j} \wedge \vec{B} = \nabla p. \tag{2.9}$$

This implies $\vec{B} \cdot \nabla p = 0$, so there is no presure gradient along the magnetic field lines, which means the magnetic surfaces are also pressure surfaces. (2.9) also implies $\vec{j} \cdot \nabla p = 0$, and as a consequence the current lie in the magnetic surfaces.

In what follows the Grad-Shafranov equation, one of the most fundamental equations of MHD equilibrium will be derived. From (2.7), taking into account the axysymmetry, and using the coordinate system of figure 2.1(a), setting $R_0 \equiv 0$,

[2] A given surface is a magnetic flux surface if it satisfies $\vec{B} \cdot \vec{n} = 0$, where $\vec{n}$ is the normal vector of the surface. That is, the magnetic field do not cross the surface. This is only a visual way to understand the magnetic field, since there would be an infinite number of magnetic flux surfaces inside a tokamak.

[3] Here an important acclaration needs to be made; MHD equations were introduced for an isolated plasma, but in tokamaks we are dealing with a plasma and coils. MHD equations are still valid, considering both the plasma and the coils as a whole system, so that $\vec{j}$ will be the current density of the plasma plus the current density of the coils, and the same applies to the electromagnetic fields.

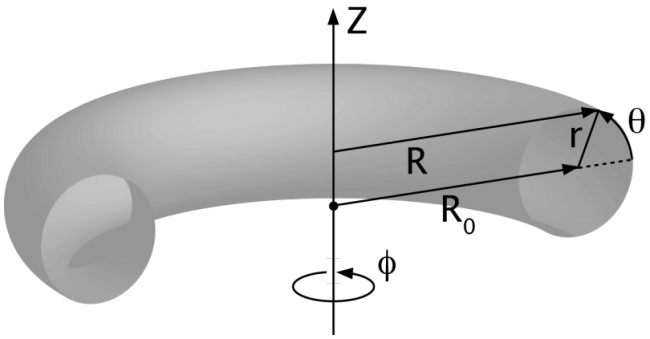

(a) Cylindrical coordinate system used in devices with torodial symmetry, (R, ϕ, Z). R_0 is called the major radius of the torus, r is called the minor radius. The circunference $R = R_0$ defines the toroidal or magnetic axis. For deriving the Grad-Shafranov equation, $R_0 \equiv 0$. Source: http://fusionwiki.ciemat.es/wiki/Toroidal_coordinates.

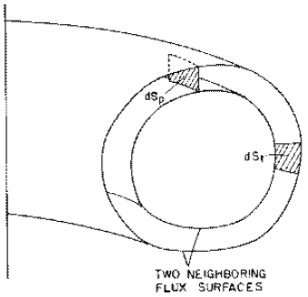

(b) Toroidal and poroidal surface elements between two magnetic flux surfaces. Source: [9].

Figure 2.1. Cylindrical coordinate system for toroidal devices, and definition of the poloidal flux in a torus.

$$\frac{1}{R}\frac{\partial(RB_{\mathrm{R}})}{\partial R} + \frac{\partial B_{\mathrm{Z}}}{\partial Z} = 0. \tag{2.10}$$

Introducing a function ψ, called the *stream function*, which verifies $\psi \equiv RA_\phi$, where A_ϕ is the toroidal component of the vector potential $\vec{A}$. With this function, the poloidal magnetic field can be written as

$$\left.\begin{aligned} B_{\mathrm{R}} &= \frac{-1}{R}\frac{\partial\psi}{\partial Z}, \\ B_{\mathrm{Z}} &= \frac{1}{R}\frac{\partial\psi}{\partial R}, \end{aligned}\right\} \Leftrightarrow \vec{B}_{\mathrm{p}} = \frac{1}{R}\nabla\psi \wedge \hat{\phi}, \tag{2.11}$$

where $\hat{\phi}$ is the toroidal unit vector (the magnetic field can be expressed as $\vec{B} = \vec{B}_{\mathrm{p}} + \vec{B}_\phi$). It can be shown[4] that $\Psi = 2\pi\psi$. It is usual to label the magnetic surfaces with ψ, also called the magnetic flux. This means that $p = p(\psi)$, since magnetic surfaces are also pressure surfaces. From the symmetry of $\vec{j}$, it can be introduced a function f that verifies

[4] See [9], section 6.2 for further details.

$$\left.\begin{aligned} j_{\mathrm{R}} &= \frac{1}{R}\frac{\partial f}{\partial Z}, \\ j_{\mathrm{Z}} &= \frac{1}{R}\frac{\partial f}{\partial R}, \end{aligned}\right\} \Leftrightarrow \vec{j_{\mathrm{p}}} = \frac{1}{R}\nabla f \wedge \hat{\phi} \tag{2.12}$$

Comparing (2.12) with (2.6) leads to

$$f = \frac{RB_{\phi}}{\mu_0}, \tag{2.13}$$

where μ_0 is the vacuum magnetic permeability and the subscript ϕ indicates the toroidal component. It can be shown that f is a function of ψ [5] .

Equation (2.9) can be expanded as

$$\vec{j_{\mathrm{p}}} \wedge \hat{\phi}\, B_{\phi} + j_{\phi}\, \hat{\phi} \wedge \vec{B_{\mathrm{p}}} = \nabla p, \tag{2.14}$$

where j_{ϕ}, $\vec{j_{\mathrm{p}}}$ is the magntiude of the toroidal current, and the poloidal current density vector respectively. Substituing (2.12) and (2.11) into (2.14), we get, using that $\hat{\phi} \cdot \nabla\psi = \hat{\phi} \cdot \nabla p = 0$ (consequence of the toroidal symmetry)

$$\frac{B_{\phi}}{R}\nabla f + \frac{j_{\phi}}{R}\nabla\psi = \nabla p. \tag{2.15}$$

To get j_{ϕ}, we substitute (2.11) on (2.6), obtaining

$$\begin{aligned} \mu_0 \vec{j} &= \mu_0 j_{\phi}\, \hat{\phi} + \frac{1}{R}\nabla(RB_{\phi}) \wedge \hat{\phi}, \\ \mu_0 j_{\phi} &= -\frac{1}{R}\nabla^{*}\psi, \end{aligned} \tag{2.16}$$

where $\nabla^{*}\psi \equiv R\nabla \cdot (\frac{1}{R}\nabla\psi) = R\frac{\partial}{\partial R}\Big(\frac{1}{R}\frac{\partial\psi}{\partial R}\Big) + \frac{\partial^2\psi}{\partial Z^2}$ is the elliptic operator. If we use the chain rule on ∇f and ∇p, and use (2.16) on (2.15), we get the Grad-Shafranov equation,

$$R\frac{\partial}{\partial R}\Big(\frac{1}{R}\frac{\partial\psi}{\partial R}\Big) + \frac{\partial^2\psi}{\partial Z^2} = -\mu_0 R^2 \frac{dp(\psi)}{d\psi} - \mu_0^2 f(\psi)\frac{df(\psi)}{d\psi}. \tag{2.17}$$

This one of the fundamental equation of MHD equilibria. It is a second order partial differential equation that calculates the equilibrium in toroidal devices, given the functions $p(\psi)$ and $f(\psi)$. In figure 2.2 (b), we can see a typical solution of this equation, showing the flux surfaces, labeled by ψ. Note that the surfaces are shifted with respect to the magnetic axis.

[5] See [1], section 2.3 .

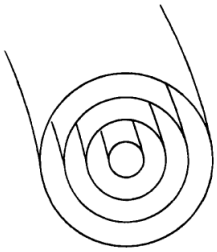

(a) Magnetic flux surfaces of a tokamak equilibria, forming a set of nested cylindrical surfaces. Source: [1].

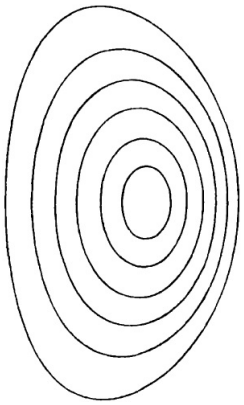

(b) Typical solution of the Grad-Shafranov equation. Source: [1].

Figure 2.2. Magnetic flux surfaces of a tokamak equilibria, and typical solution of the Grad-Shafranov equation.

2.3 Tokamaks parameters

It is needed to introduce the most important parameters of a tokamak equilibria, as well as about plasma shape and control to understand this work.

2.3.1 Plasma shape and control in tokamaks

The first concept it has to be introduced is the plasma boundary. The boundary of the plasma is the outermost closed magnetic surface contained in the vessel. Particles inside this outermost surface follow the field lines that remain in the plasma, but particles that follows the external field lines will end up scaping form the plasma[6], and colliding with the vessel. The boundary can be created by a set of coils, or it could be the vessel. The first method create the outermost closed magnetic surface displaying one or more *X-points*. X-points are saddle points where $\frac{\partial \psi}{\partial Z} = \frac{\partial \psi}{\partial R} = 0$, so the poloidal magnetic field is zero (see (2.11)). The outermost closed surface is called *separatrix*, and the plasma confined this

[6]Particles follows the magnetic field lines, but if the external magnetic field lines are not closed inside the vessel, particles will collide with the vessel.

way is called diverted plasma, and the coils used to create it are called divertor coils. The second method is to limit the plasma by the vessel, so that the plasma is touching the vessel. The plasma is then called *limited plasma*. In figure 2.3 (a) a limited plasma and a diverted plasma with one X-point is showed. The Seville ST will contain a diverted plasma with two X-points[7]

For shape control of the plasma, the following paramentes are introduced to describe the shape of the last closed surface, with the points defined in figure 2.3 (b) [8] :

$$\begin{array}{cc} \text{Major radius} & R_{\text{geo}} \equiv (R_{\max} + R_{\min})/2, \\ \text{Minor radius} & a \equiv (R_{\max} - R_{\min})/2, \\ \text{Aspect ratio} & A \equiv R_{\text{geo}}/a, \\ \text{Elongation} & \kappa \equiv (Z_{\max} - Z_{\min})/(2a), \\ \text{Upper triangularity} & \delta_{\text{u}} \equiv (R_{\text{geo}} - R_{z_{\max}})/a, \\ \text{Lower triangularity} & \delta_{\text{l}} \equiv (R_{\text{geo}} - R_{z_{\min}})/a. \end{array} \tag{2.18}$$

2.3.2 q and β factors

The confinement efficiency of the plasma in a tokamak is represented by β, which is the ratio between the average pressure of the plasma p and the energy density stored in the magnetic field, or magnetic pressure,

$$\beta \equiv \frac{p}{\frac{B^2}{2\mu_0}}. \tag{2.19}$$

Note it is a dimension-less magnitude. β defines the confinement efficiency because given a plasma with a certain average pressure, it determines the magnetic field necessary to confine it. As a consequence, a high value of β is attempted. This also leads to the definition of poloidal β,

$$\beta_{\text{poloidal}} \equiv \beta_{\text{p}} \equiv \frac{\int_{S_{\text{p}}} p dS_{\text{p}} / \int_{S_{\text{p}}} dS_{\text{p}}}{B_{\text{a}}^2/2\mu_0}, \tag{2.20}$$

where $B_{\text{a}} \equiv \mu_0 I/l$, I is the plasma current and l is the poloidal perimeter. The toroidal beta β_{t} is defined in a similar way. It is also define the so called *normalized beta* β_{N}, which is also a dimension-less magnitude, as

[7] See figure 5.1 to see the equilibrium configuration studied in this thesis.

[8] See [10] for further details.

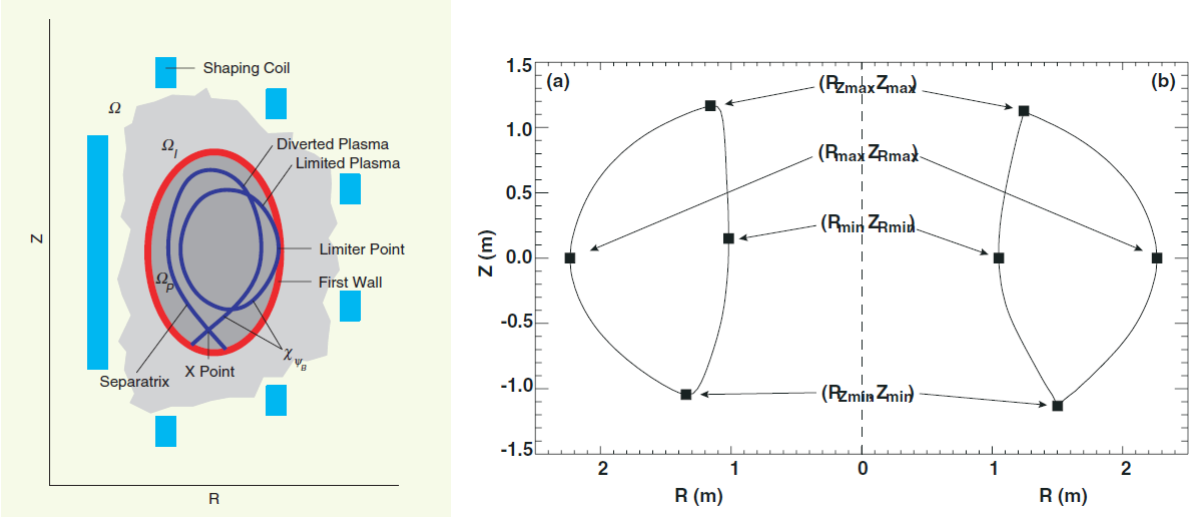

(a) Cross-section of a tokamak, showing its coils, and the boundaries (in dark blue) of a diverted plasma, a plasma whose boundary is made by coils that creates the last closed magnetic surface, which displays one X-point and a limited plasma, a plasma that touches the vessel of the tokamak (in orange). Source: [4].

(b) Contour of the last close surface of a limited plasma (left) and a diverted plasma (right), showing the points used to describe the plasma shape. Source: [10]

Figure 2.3. Plasma geometry and plasma boundaries in tokamaks

$$\beta_{\mathrm{N}} \equiv \frac{\beta_{\mathrm{t}} B_{\mathrm{T0}} a}{I_{\mathrm{p}} \mu_0}, \tag{2.21}$$

where B_{T0} is the toroidal field at plasma geometric centre, commonly label simply as B_{T} and I_{p} the plasma current.

Another relevant parameter is the *safety factor* q, which determines the stability of the plasma, higher values of q leads to greater stability. Each magnetic flux surface has its value, and its value is related to the helical paths of the field lines. If at a certain toroidal angle ϕ the field line has a certain position in the poloidal plane, and it returns to the same position in the poloidal plane after a change of the toroidal angle $\Delta\phi$, the q factor is

$$q \equiv \frac{\Delta\phi}{2\pi}. \tag{2.22}$$

As a conquence of this definition, lower values of q leads to more squeezed helical magnetic

field lines, which result in better confinement. $q = 1$ means that the magnetic field line returns to its initial position after one rotation around the torus. If $q = \frac{m}{n}$, where m and n are integers, it means that the field line returns to its initial position afer m toroidal rotations and n poloidal rotations round the torus. For an exact calculation it is necessary to use the field line equation,

$$\vec{B} \wedge \vec{dr} = 0 \Rightarrow \frac{B_\phi}{Rd\phi} = \frac{B_\mathrm{p}}{dl_\mathrm{p}}, \tag{2.23}$$

where $\vec{dr}$ is a differential vector lying on the field lines, $Rd\phi$ is the toroidal line element, and dl_p is the poloidal line element so moving $Rd\phi$ in the toroidal directions means moving dl_p in the poloidal direction. Introducing (2.23) in (2.22) it is obtained the general formula to obtain the safety factor

$$q = \frac{1}{2\pi} \oint_{l_\mathrm{p}} \frac{1}{R} \frac{B_\phi}{B_\mathrm{p}} dl_\mathrm{p} \tag{2.24}$$

where the integral is carried out over the boundary of the poloidal surface of the magnetic flux surface, showed in figure 2.4. From this definition, the safety factor is a function of the poloidal flux ψ, since it is obtained integrating over a magnetic flux surface, which, as said previously, is label by ψ. The safety factor can also be expressed as

$$q = \frac{d\Phi}{d\Psi}. \tag{2.25}$$

It is usual to plot the safety factor as a function of the normalized poloidal flux, defined as

$$\psi_\mathrm{N} \equiv \frac{\psi - \psi_\mathrm{axis}}{\psi_\mathrm{boundary} - \psi_\mathrm{axis}}, \tag{2.26}$$

where ψ_axis and ψ_boundary are the values of the poloidal flux at the center of the magnetic flux surface and at its boundary. This plot is called *q profile*. When a plasma is bounded by a separatrix, the q profile is modified in the proximity of the X-point, where $q \to \infty$, since at this point the poloidal field is zero, so the magnetic field lines are horizontal. Figure 2.5 shows the q profile of one of the set-ups of the Seville ST studied in this thesis, called V2C2, and a plot of the value of ψ_N as a function of R over the plasma region, displaying the geometric centre of the plasma R_geo with a red dot.

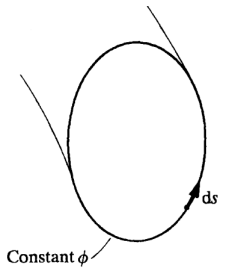

Figure 2.4. Integration path for the calculus of the safety factor. It is shown a magnetic flux surface, displaying a cros-section with a constant value of the toroidal angle ϕ, and the line element $ds \equiv dl_\mathrm{p}$. Source: [1].

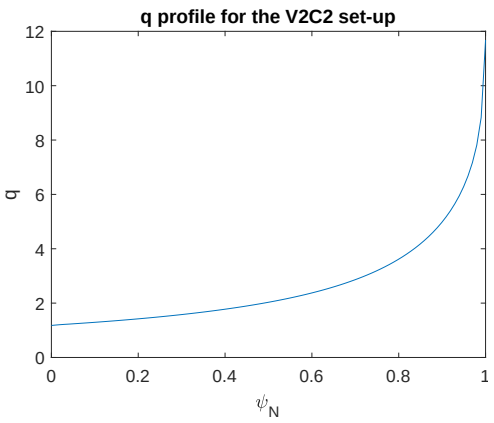

(a) q profile. Note that q increases rapidly as approaching the outermost closed surface contained in the vessel due to the presence of X-points in this surface.

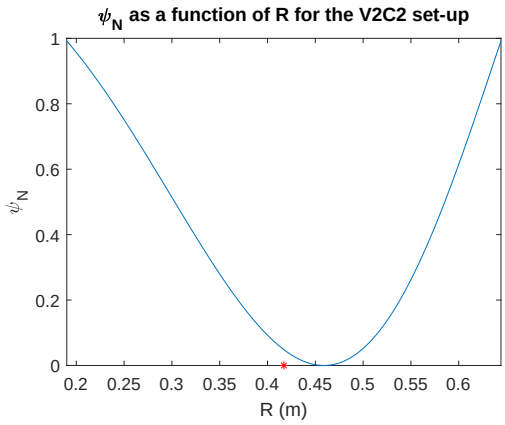

(b) ψ_N versus R in the plasma region. The red point indicates R_{geo}.

Figure 2.5. q profile and ψ_N as a function of the radial coordinate R for one of the set-ups of the Seville ST studied in this thesis. All the configurations displays two X-points.

Making use of the parameters defined above, the fusion or thermonuclear power can be written as[9]

$$P_{fus} \propto \beta_N^2 \kappa (1+\kappa)^2 \frac{R_{geo}^3 B_{max}^4}{q(a)^2} \frac{f(A)^2}{(A+1)^4 A^2}, \tag{2.27}$$

where B_{max} is the maximum toroidal magnetic field, $f(A) \equiv 1.22A - 0.68$, and $q(a)$ is the safety factor at the plasma boundary. From this formula, increasing κ leads to greater fusion powers, which is one of the advantages of spherical tokamaks.

[9] See [11] for further details.

Chapter 3

FIESTA code

In this chapter the numerical tools used in this thesis are introduced.

3.1 FIESTA code

The FIESTA code is an object-oriented code programmed in MATLAB that solves the equilibrium configuration of a plasma, and computes the time response of a tokamak.

The calculation of the eddy currents is a key factor for the vessel design, since it provides information about the temperature of the vessel (by Joule's heating law), the mechanical forces acting upon the vessel and about the real magnetic field inside the vessel, as said previously. The vessel has eddy current because of the current changes, either in the plasma or in the coilset. A current change leads to a magnetic field change, which leads to the creation of an electromotive force, according to Faraday's law, (2.5). FIESTA approximates the vessel as a set of filaments, so (2.5) in its integral form can be aplied,

$$\oint_{\partial S} \vec{E}_{\text{eddy}} \cdot \vec{dl} = -\iint_S \frac{\partial \vec{B}}{\partial t} \cdot \vec{n} dS = -\frac{\partial}{\partial t} \iint_S \vec{B} \cdot \vec{n} dS, \tag{3.1}$$

where $\vec{E}_{\text{eddy}}$ is the induced electric field, $\vec{B}$ the total magnetic field, S a surface enclosed by the circular wires, ∂S the boundary of S, and $\vec{n}$ the normal vector of the surface S. For the last step of (3.1) it has been taken into account that the surface does not vary with time. This equation means that the change of the total flux (the sum of the poloidal and toroidal flux) induces an electromotive force on the wires. The sign of the eddy current can be deduced by the Lenz's law (although it is already indicated in the negative sign),

which states that the induced current is in such a direction as to oppose the change of magnetic flux.

FIESTA, as an object-oriented programming code, is characterized by the hierarchy of its elements. Figure 3.1 shows a schematic graph of class dependencies for the FIESTA code. The simplest conductor of FIESTA is a filament. To create it, the center position, the width and heigh and the number of turns of the filament are needed. The filaments can be grouped either in a coil or a passive. These clases both defines the resistivity of the set of filaments. The difference between them is that in a coil the filaments are connected in series, while in a passive they are not connected. The passives are used to create the vessel, which can be composed of one or more passives. The coils are grouped in circuits. The polarity of the connection of the coils, in series (+1) or in parallel (-1) needs to be introduced. Poloidal field coils and the inductor solenoid are fiesta_circuits. The circuits are then group in a coilset. Finally, the circuits and their currents are group in an icoil.

Grad-Shafranov equation is solved by an iterative method, according to a given tolerance. A plasma model needs to be defined to solve it. It have been used the Topeol type 2 model, which defines the functions $p(\psi)$ and $f(\psi)$ as

$$\begin{cases} \dfrac{dp}{d\psi} = \dfrac{j_0}{r_0}\beta_{\mathrm{p}}(1-\psi_{\mathrm{N}}), \\ f\dfrac{df}{d\psi} = \mu_0 r_0 j_0 (1-\beta_{\mathrm{p}})(1-\psi_{\mathrm{N}}), \end{cases} \tag{3.2}$$

where r_0 is the X-point radial coordinate and j_0 the plasma current. Both parameters are adjusted at each step of the iterative process. The grid where FIESTA will solve Grad-Shafranov equation needs to be defined. With the grid, the Green's function of the coilset will be calculated. Green's functions are used to compute the magnetic field.

FIESTA solves the RZIP model, to get the time response of the system. To solve it, the coilset current profile have to be introduced (i.e., the ramp up and down of the coils, achieving the current used in the equilibrium calculation). The ouputs are the plasma current and voltage, the coilset voltage and the eddy currents in the vessel.

The FIESTA code is very complex, on the order of hundreds of thousands of code lines. Furthermore, in spite of its neat object hierarchy, it is scarcely documented, so direct code reading is imperative. However, for this thesis it is sufficient to understand the basis of the FIESTA code as described above.

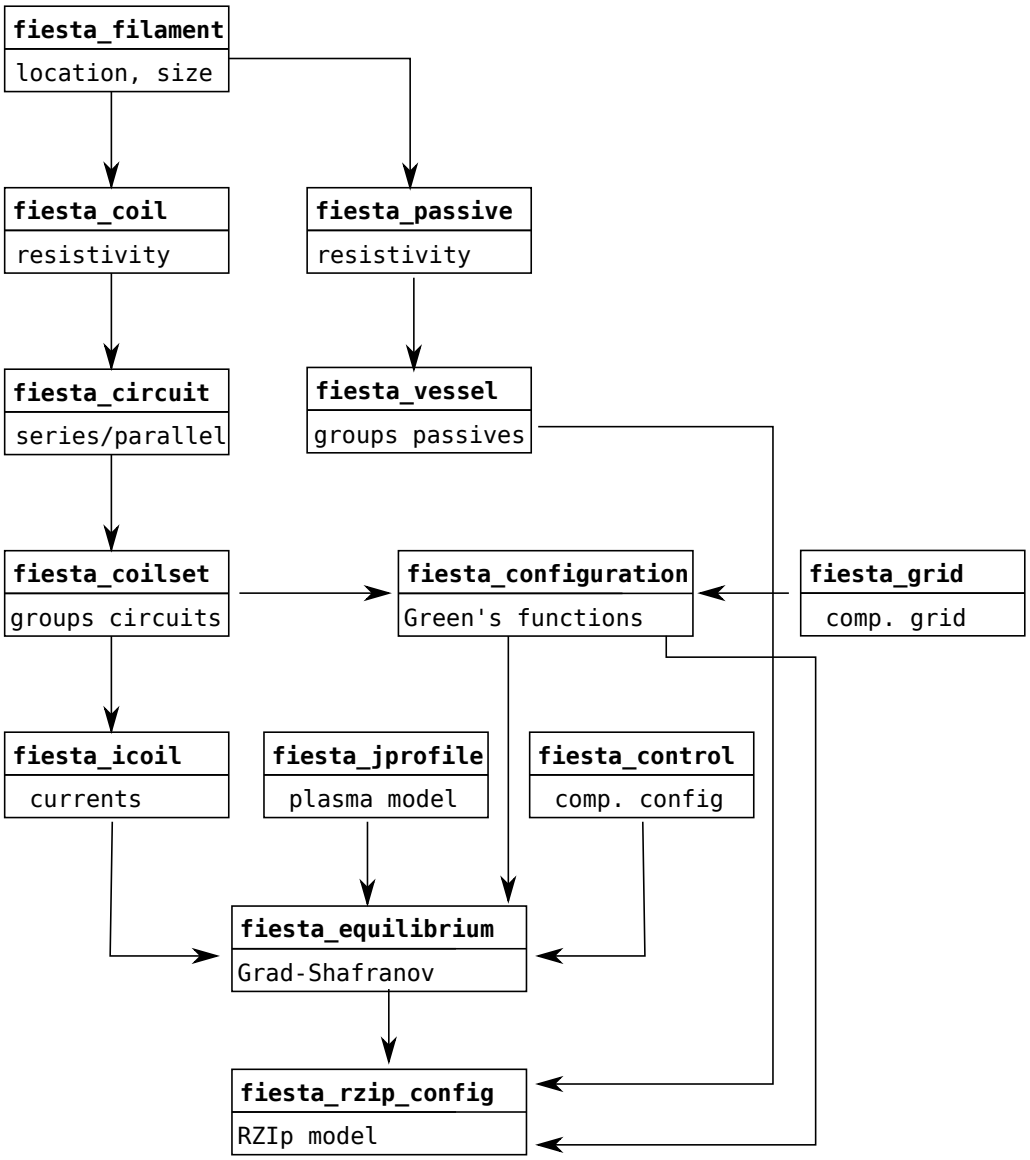

Figure 3.1. Schematic graph of class dependencies for the FIESTA code, restricted to the subset of classes used for this thesis. Only the name and main physical data are displayed for each class. The dependencies shown in this graph do not necessarily involve class inheritance. Comp. means computational.

3.1.1 RZIp model

The rigid current displacement model, or RZIp (R, Z and I_p), is a model used to describe the dynamic behaviour of a tokamak equilibria, considering the plasma a rigid conductor in the sense that it can move radially and vertically, but the plasma current distribution remain constant[1], so the plasma is identified by its radial and vertical position, R and Z, and its current, I_p. It is a linearised code based on the premise that small perturbations leads to small changes of the equilibria. Its equations are the circuit equation, and the radial and vertical force balance equations.

This model consideres that a tokamaks is made of active and passive elements. An element is considered an active element if is subjected to a external excitation such as current or voltage supplies and passive in any other case. The active structure will then be the coilset, and the passive structure the vessel. If there is no plasma, the circuit equations is

$$\boldsymbol{M}_\mathrm{c}\frac{d\boldsymbol{I}_\mathrm{c}}{dt} + \boldsymbol{\Omega}_\mathrm{c}\boldsymbol{I}_\mathrm{c} = \boldsymbol{V}_\mathrm{c}, \tag{3.3}$$

where $\boldsymbol{M}_\mathrm{c}$ is the inductance matrix between the active structure and the vessel, $\boldsymbol{I}_\mathrm{c}$ is a row vector containing the PF coil curents, $\boldsymbol{V}_\mathrm{c}$ contains their voltages, and $\boldsymbol{\Omega}_\mathrm{c}$ is the resistance matrix, which is a diagonal matrix. This is just the circuit equation for a set of inductive and resistive elements. If the plasma is considered, the circuit equation becomes

$$\boldsymbol{M}_\mathrm{c}\frac{d\boldsymbol{I}_\mathrm{c}}{dt} + \left(\frac{\partial \boldsymbol{M}_\mathrm{c}}{\partial R}\right)^T I_\mathrm{p}\frac{dR}{dt} + \left(\frac{\partial \boldsymbol{M}_\mathrm{c}}{\partial Z}\right)^T I_\mathrm{p}\frac{dZ}{dt} + \boldsymbol{M}_\mathrm{p}^{\boldsymbol{T}}\frac{dI_\mathrm{p}}{dt} + \boldsymbol{\Omega}_\mathrm{c}\boldsymbol{I}_\mathrm{c} = \boldsymbol{V}_\mathrm{c}, \tag{3.4}$$

where $\boldsymbol{M}_\mathrm{p}$ is the inductance between the plasma and the active structure and ^{T} is the transpose operator.

The vertical force balance equation is, neglecting the plasma mass,

$$\frac{\partial \boldsymbol{M}_\mathrm{c}}{\partial Z}\boldsymbol{I}_\mathrm{c} - \alpha Z I_\mathrm{p} = 0, \tag{3.5}$$

where $\alpha \equiv -(2\pi R_0/I_{\mathrm{p}0})(\partial B_\mathrm{R}/\partial Z)|_{Z=Z_0}$, where the subscript 0 indicates the equilibrium value.

[1] There are many articles about the RZIp model, such as [12] or [13]. FIESTA implements a code in a similar way as explained in [13], and the approach given in this article is going to be resumed. [12] tries to set a robust mathematical basis of the RZIP code, but it is not the version FIESTA uses. Also, it can be seen [14] for a general description of several tokamak codes.

The perturbed radial force balance equation is expressed by the time derivative of its linearized variation

$$\frac{d}{dt}(\delta \sum F_{\mathrm{R}}) = \frac{d}{dt}[\delta(2\pi R I_{\mathrm{p}} B)] = 0 \tag{3.6}$$

The set of equations (3.4), (3.6) and (3.5) can be written in the form

$$\boldsymbol{M}\frac{d\boldsymbol{x}}{dt} + \boldsymbol{\Omega}\boldsymbol{x} = \boldsymbol{u}, \tag{3.7}$$

where $\boldsymbol{x}$ is

$$\boldsymbol{x} = \begin{bmatrix} \boldsymbol{I}_{\mathrm{c}} \\ Z I_{\mathrm{p0}} \\ R I_{\mathrm{p0}} \\ I_{\mathrm{p}} \end{bmatrix} \tag{3.8}$$

The equation (3.7) can be cast in the state-space model form, whose general structure is [2]

$$\begin{cases} \dfrac{d\boldsymbol{x}}{dt} = \boldsymbol{A}\boldsymbol{x} + \boldsymbol{B}\boldsymbol{u}, \\ \boldsymbol{y} = \boldsymbol{C}\boldsymbol{x} + \boldsymbol{D}\boldsymbol{u}, \end{cases} \tag{3.9}$$

and comparing the state space general structure with (3.9):

$$\begin{aligned} A &= -\boldsymbol{M}^{-1}\boldsymbol{\Omega}, \\ B &= \boldsymbol{M}^{-1}. \end{aligned} \tag{3.10}$$

The RZIp model is solved on FIESTA by solving the state-space problem, such that it calculates the time evolution (or dynamic response) of the plasma current, the plasma and coilset voltages and the eddy current induced on the vessel, given an initial current profile of the coilset.

[2] See appendix A for further details about state space representation

Chapter 4

Experimental method

As a first approach to the search of the best scenario for the future Seville ST, four differents tokamak configurations have been studied exploring and comparing them using the FIESTA code. Figure 4.2 shows the cross-section of the four configurations studied, named V1C1, V1C2, V2C2 and V2C3. Note all the configurations are symmetric with respect to the $Z = 0$ plane. Figure 4.1 shows a 3D plot of the vaccum vessel (grey) and the coilset (blue) of the V1C1 set-up, labeling each coil pair.

In order to do that comparison, extensive simulations were carried out to achieve similar equilibria (i.e., the solution of Grad-Shafranov equation). Having similar target equilibria, the coilset current needed to achieve it could be compared, as well as the time response of the tokamak, the eddy currents in the vessel and the pressure the vessel has to withstand.

The magnetic forces on the vessel are another key parameter for the vessel design, because this forces could lead to the destruction of vessel. The forces can be calculated by taking into account that FIESTA decomposes the vessel in a set of filaments. As a consequence, in order to

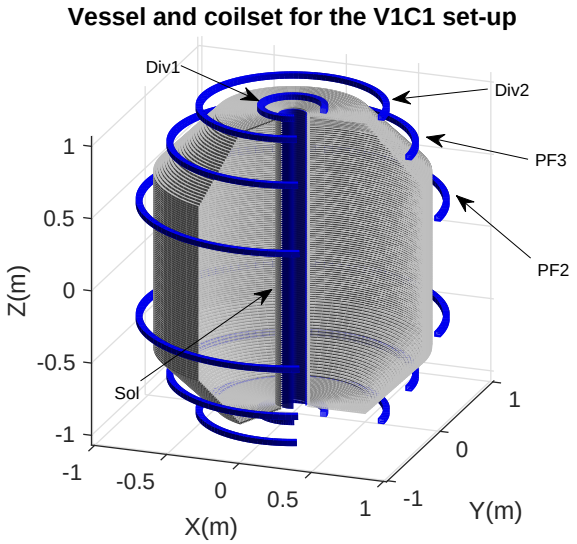

Figure 4.1. Vacuum vessel (grey) and coilset of the V1C1 configuration (blue), displaying the names of each pair of coils (all the configurations displays simmetry with respect to the $Z = 0$ plane) and the inductor solenoid.

compute the force, the widely known equation of the magnetic force ating upon a wire, introduced in figure 1.6, can be used,

$$\vec{F}_{\text{mag}} = \int_{\Gamma} I\vec{dl} \wedge \vec{B} \tag{4.1}$$

where the integral is carried out on the wire length Γ, I is the current carried by the wire, $\vec{dl}$ is the differential element of the wire, whose direction is the direction of the current I, and $\vec{B}$ the magnetic field. $\vec{dl} = Rd\phi$, where ϕ is the toroidal angle, and, since the system displays toroidal symmetry, the force upon each filament of coordinates R_{fil} and Z_{fil} is

$$\vec{F}_{\text{mag}}(R_{\text{fil}}, Z_{\text{fil}}) = 2\pi R_{\text{fil}} I[B_{\text{Z}}(R_{\text{fil}}, Z_{\text{fil}}) \hat{R} - B_{\text{R}}(R_{\text{fil}}, Z_{\text{fil}}) \hat{Z}], \tag{4.2}$$

where $B_{\text{R}}(R_{\text{fil}}, Z_{\text{fil}})$ and $B_{\text{Z}}(R_{\text{fil}}, Z_{\text{fil}})$ are the radial and vertical components of the magnetic field evaluated at the filament's coordinates.

In order to do the comparsion to select the best scenario the following aspects must be taken into consideration:

- Equilibrium parameters such as the safety factor and β, and also geometric parameters such as the elongation. Low q means high confinement, high β means high confinement efficiency, as said in section 2.3.2. High elogation leads to greater fusion power[1].
- Coilset currents.
- Eddy currents. Low eddy current means low forces on the vessel, which also means low mechanical stresses under the vessel, and low shielding of the magnetic field created by the coilset.

Table 4.1 displays the parameters of the simulations carried out, where $\tau \equiv \tau_{\text{e}}$ is the discharge or confinement time, i.e., the time the plasma is sustained with the desired current, in this case, 100kA.

To achieve a similar equilibria in all the configurations, scans in coil currents and positions has been run, keeping fixed the rest of parameters such as their turns and size.

[1]The Seville ST will not be a fusion power plant, but it is convenient to study hihgly elongated plasmas because they are the most convenient plasmas to use in a fusion power plant, as said at the end of section 2.3.2.

The VEST tokamak has been used as a reference for the scans[2]. Table 4.2 shows the coilset parameters for the differents set-ups. Note that the radial distance between Div coils is the same for all the configurations, as well as their position. This is because it has been found that this position is optimal to reduce the applied currents, as well as to reduce the safety factor q. Moreover, V1C1 and V2C1 displays the same coil configuration, so its comparison would provide relevant information about the optimal shape of the vessel. On the other hand, V2C1 and V2C3 includes coils inside the vessel. The coils are closer to the plasma in order to decrease the currents needed (the magnetic field decreases with distance), but it must be checked if this is worthwhile, because it may increase another relevant parameters such as the eddy currents or the safety factor.

Vessel	Height(m)	2.0
	Diameter(m)	1.6
	Wall thickness(m)	0.015
Plasma	I_{p}(kA)	100
	$\eta_{\mathrm{p}}(\Omega\cdot$ m)	$0.5 \cdot 10^{-6}$
B_{T}(T)		0.3
τ(ms)		100
Coil temperature(K)		293

Table 4.1. Parameters of the simulations carried out. The value of the plasma resistivity η_{p} and the coil temperature has been arbitrarily set. Note the plasma density and temperature has not been used in the simulation since they only play the role of determining the plasma resistivity (Spitzer resistivity), and this value has been set.

[2]The first plasma discharge of the VEST ST is shown in[15], where it is also shown its cross-section.

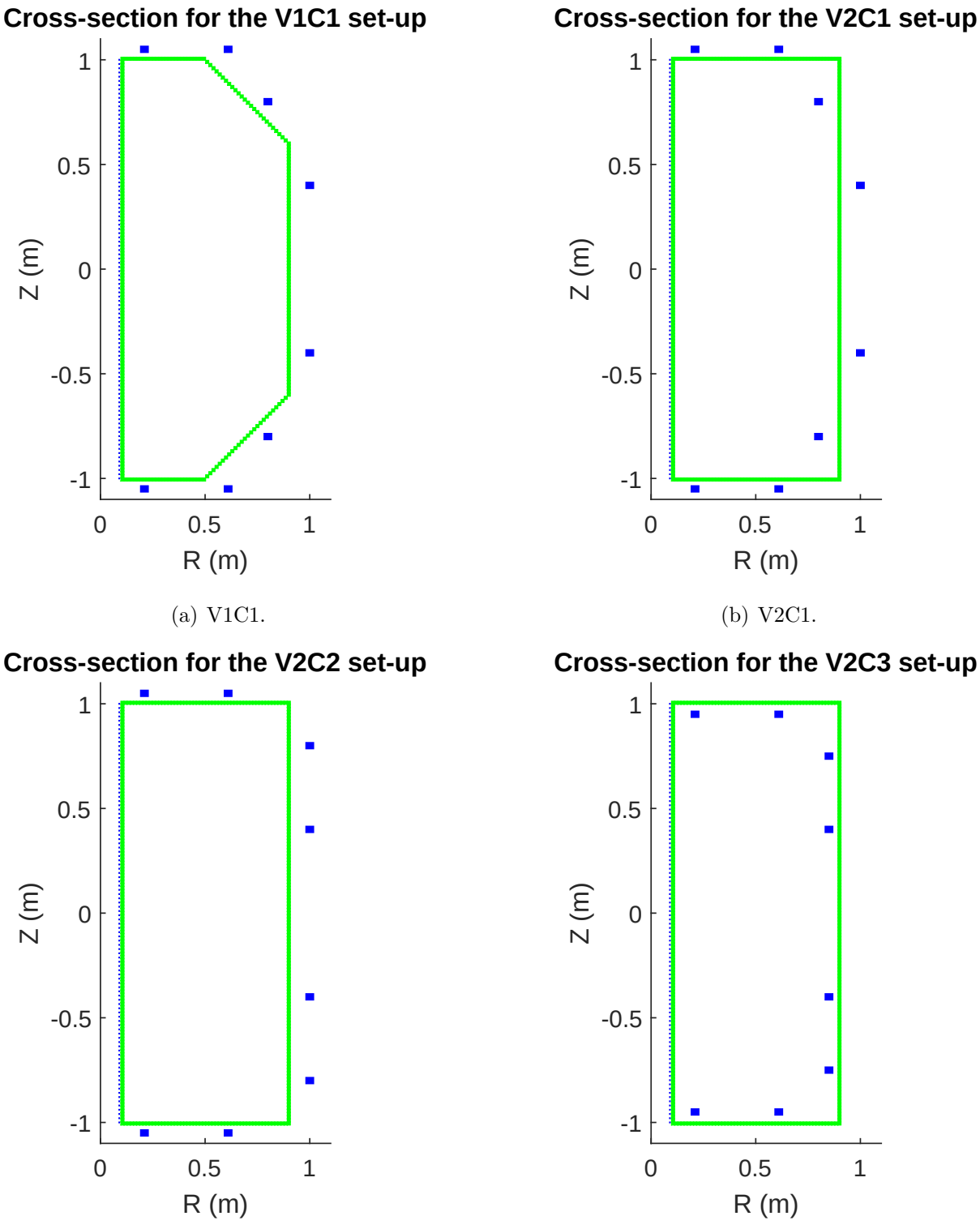

(a) V1C1.

(b) V2C1.

(c) V2C2.

(d) V2C3.

Figure 4.2. Cross-section of the different configurations explored in this thesis. The vaccum vessel is green coloured and the coilset, made by the PF cand Div coils and the inductor solenoid, Sol, is shown in blue. The solenoid is the linear array of blue dots next to the inner side of the vessel.

	Sol		Div1		Div2		PF2		PF3	
Turns	100		8		8		24		24	
Height(m)	2.0		0.035							
Width(m)	0.0084		0.042							
coil center position										
	R(m)	Z(m)	R(m)	Z(m)	R(m)	Z(m)	R(m)	Z(m)	R(m)	Z(m)
V1C1	0.09	0.0	0.21	1.095	0.61	1.095	1.0	0.4	0.8	0.8
V2C1			0.21	1.095	0.61	1.095	1.0	0.4	0.8	0.8
V2C2			0.21	1.095	0.61	1.095	1.0	0.4	1.0	0.8
V2C3			0.21	0.895	0.61	0.895	0.85	0.4	0.85	0.75

Table 4.2. Coilset parameters of the differents configurations studied. The coilset size and number of turns have been set according to the VEST's design parameters, and the coilset position of the different configurations have been selected after selective scans.

Chapter 5

Results

In this chapter the results of the simulations introduced in the previous chapter are reported and discussed. The target equilibria for all the set-ups is shown in figure 5.1, displaying the vessel (green), the coilset (blue, though it is difficult to see it), the contour of the poloidal flux lines, and the last closed surface inside the vessel with a thicker line, where the plasma is confined. The coilset can also be identifyed by seeing the accumulation of flux lines, which also indicates the current on the coil, since larger currents leads to more line accumulation.

The coilset currrent is displayed in table 5.1. The currents are given in MA · turn, in order to make the results obtained independent of the number of turns[1]. Note the Sol current needed to achieve the desirable plasma current is also included. However, for the equlibrium calculation its current is zero, since the solenoid is turned off to create the plasma current. It can be easily noticed that the coilset current for the V1C1, V2C1 and V2C2 configurations are the same. It is reasonable that the V1C1 and V2C1 set-ups displays the same currents, provided that their coilset are in the same position, and the vessel do not play any role on the equilibrium calculation[2]. In the V2C2 set-up, the PF3 coil is introduced inside the vessel, but its current can not be reduced. The reason is that if it is reduced, the PF2 coil current has to be increased to keep the plasma close to the left side of the cross-section of the vessel, and since the PF2 coil current is greater than PF3 coil current, it has not been modified. The V2C3 set-up indeed requires a modification of the PF2 and PF3 coil currents, as well as a modification in the Sol current.

[1]The same current · turn value could be achieved by modifying the number of turns and the current flowing through the coil, but the product needs to reamin constant to achieve the equilibria showed here.

[2]This can be easily understood by seeing figure 3.1.

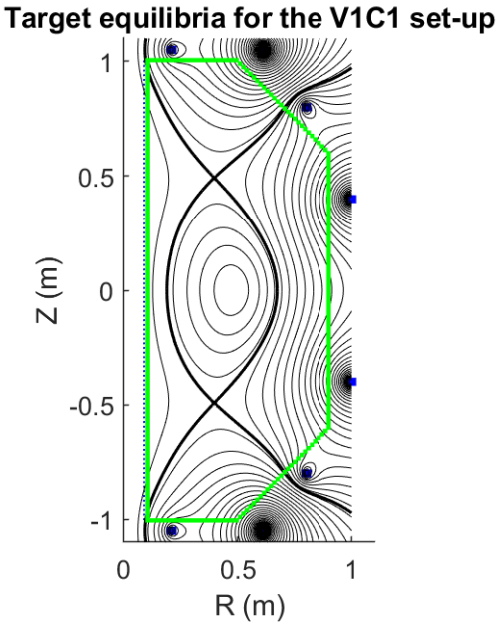

(a) V1C1.

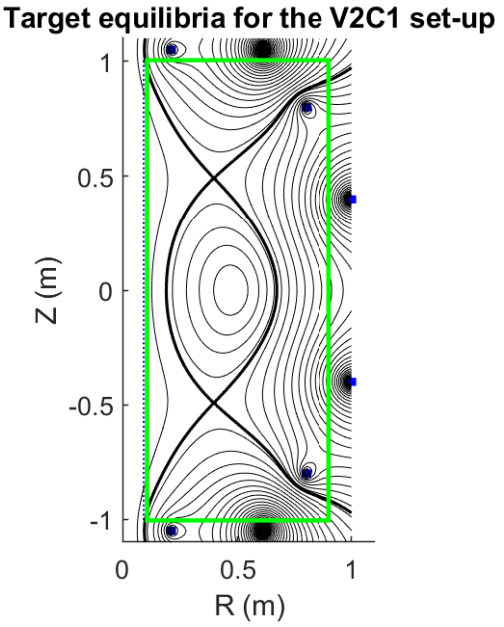

(b) V2C1.

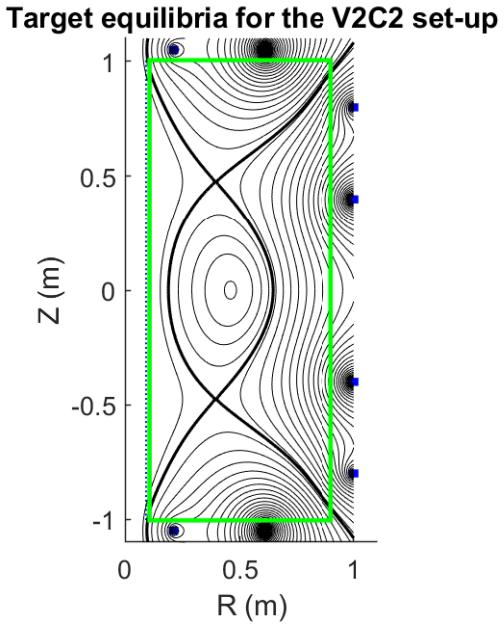

(c) V2C2.

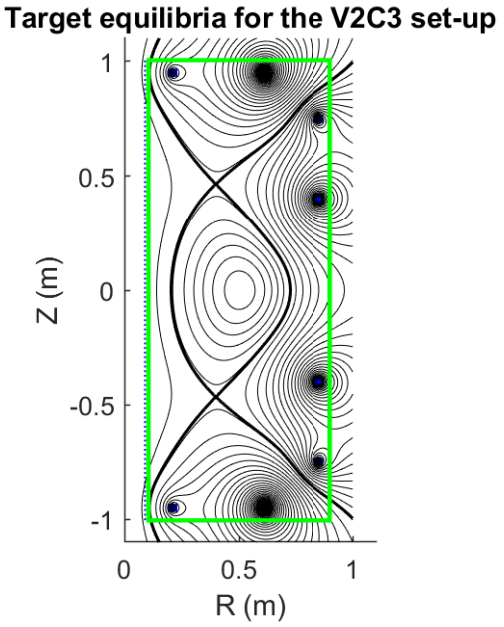

(d) V2C3.

Figure 5.1. Target equilibria for the different configurations. The vessel is shown in green, the coilset is shown in blue (although it is difficult to see it), the contour lines are poloidal flux ψ lines, and the thicker line is the outermost closed surface inside the vessel, i.e., the separatrix, displaying two X-points (consequence of the symmetry with respect to the $Z = 0$ plane). The position of the coils can be easily identified by the accumulation of flux lines, forming a black point, which also indicates the intensity of the coil, since greater intensity means a greater accumulation of flux lines. The plasma is located inside the outermost closed surface inside the vessel. It has been tried to achieve similar target equilibrias for all the configurations.

Coil name	Coil current (MA · turn)			
	V1C1	V2C1	V2C2	V2C3
Div1	0.100			0.080
Div2	0.110			0.090
PF2	-0.050			-0.045
PF3	-0.030			-0.030
Sol	2.500			3.000

Table 5.1. Coilset current used to achieve the target equilibria shown in figure 5.1. It is also included the solenoid current needed to achieve I_p=100kA, despite it has to be noted that for the equilibrium calculation the solenoid has no current, since it is turned off to create the plasma current. This is why its row in the table has two horizontal lines.

The equilibrium parameters are shown in table 5.2. This table displays some of the parameters introduced in sections 2.3.1 and 2.3.2, as well as some other parameters such as the major Z value, Z_{geo}, defined in a similar way to R_{geo}, or $q95$ and $q0$, which are the safety factor at the surface with ψ_N=0.95 and 0 respectively. The plasma energy is also shown. Figure 5.2 shows the q profile of all the configurations studied (figure 2.5 shows ψ_N as a function of the radial coordinate R for the V2C2 set-up, although all the set-ups have similar graphs). All the set-ups displays the same behaviour, with similar values, but the V2C3 set-up has the lowest values.

To obtain the time response of all the set-ups, the current profile given as a input is shown in figure 5.3. The current profile shows an standard tokamak start-up. Firstly, the current on the inductor solenoid is stablished, and in $t = 0$ the current is decreased, so that it induces a current in the plasma (it is asumed that the plasma is created on $t = 0$). At the same time, the PF and Div coils are turned on to create the magnetic field that confines the plasma. To sustain the plasma with the same current during the confinement time, the Sol current must keep decreasing. After the confinement time, 100ms, all the coils are turned off.

Figures 5.4 and 5.5 show the time response of the different configurations. The upper graphs shows the coilset current in kA (in figure 5.3 it is shown in MA · turn) and the plasma current. The central graph displays the voltages of both the coilset and the plasma, and the last graph shows the total eddy current in the vessel, $I_{passive}$, which is the sum of

Parameter	V1C1	V2C1	V2C2	V2C3
R_{geo}(m)	0.432	0.431	0.417	0.465
Z_{geo}(m)	0	0	0	0
A	1.802	1.800	1.837	1.798
κ	1.919	1.921	1.955	1.683
δ	0.138	0.150	0.116	0.249
$q95$	6.409	6.671	6.302	5.448
$q0$	1.191	1.240	1.187	0.995
β_{T}	0.0189	0.017	0.019	0.023
β_{p}	0.452	0.446	0.474	0.470
β_{N}	0.013	0.012	0.013	0.017
Plasma energy(kJ)	0.774	0.760	0.7.84	0.902

Table 5.2. Equilibirum parameters of the different configurations. Due to the symmetry with respect to the $Z = 0$ plane, the value Z_{geo} is zero.

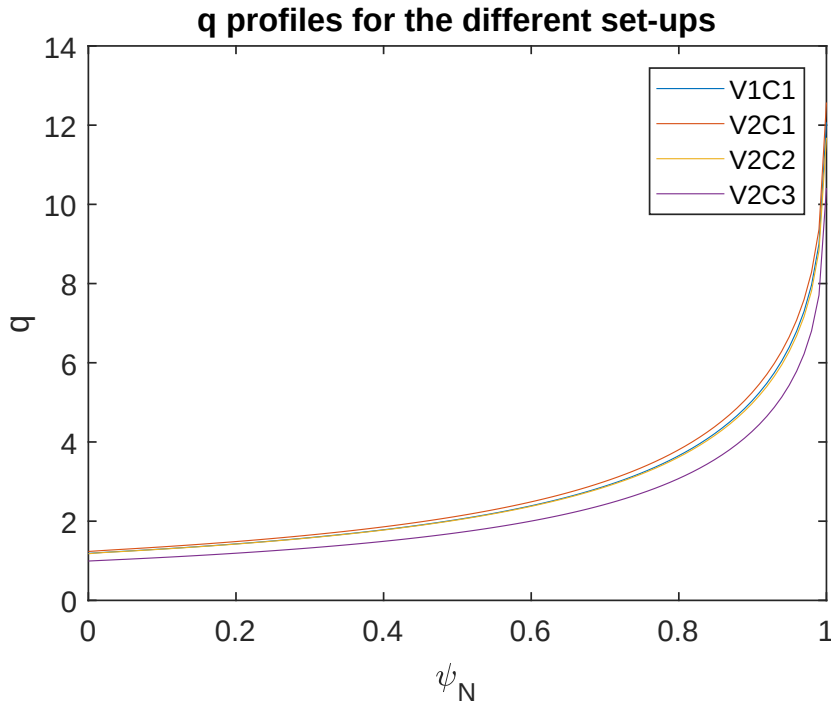

Figure 5.2. q profiles of the four configurations studied. In this graph it can also be seen $q95$ and $q0$, since the first is the q value when ψ_{N}=0.95, and the second one when it is zero. Note that the safety factor increases rapidly as approaching the outermost closed surface contained in the vessel, as expected due to the existance of two X-points.

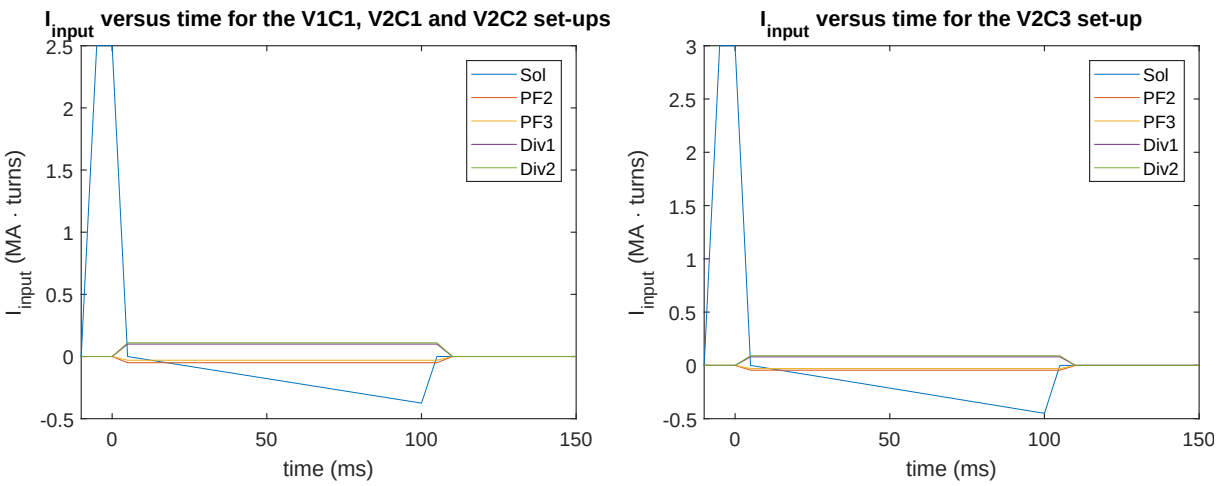

(a) V1C1, V2C1 and V2C2.

(b) V2C3.

Figure 5.3. Current profile given as an input for the time-response calculation of the Seville ST. The profile displays the standard form of a tokamak discharge. The current of the inductor solenoid, Sol, is stablished at $t < 0$, and at $t = 0$ it is decreased, so that it induces a current in the plasma. Also at $t = 0$ the Div and PF coil currents are turned on to create the field that confines the plasma. To sustain the plasma during a time interval of 100ms, the Sol current has to be decreasing during this time interval. Finally, all the coils are turned off.

the eddy currents induced in every vessel's filament. In the upper graph it can be seen that in $t = 0$ the plasma is started, an its current rises up to 100 kA, as desired. To maintain this value during the confinement time, the Sol current must keep decreasing. After this time interval, the coilset is turned off. The plasma current has decreased to half of its initial value, and then it slowly decreases. It has not been possible to ramp the plasma current down to zero by variations of the coilset current, so others method of terminating the plasma discharge needs to be studied. The last graph displays the expected behaviour, eddy currents is created when any current magnitude is changing, so there is a net variation of the magnetic flux. The Sol coil induces negative current when it is turned on, so when it is turned off it induces positive curret. However, it can be noticed than the magnitudes of the eddy current is not the same when Sol is turned on and off, and it is because of the PF and Div coils, which reduce the eddy current when the Sol coil is turned off. Therefore, the inductor solenoid plays the dominant role on the creation of eddy currents.

It can be seen that the V1C1, V2C1 and V2C2 set-ups have very similar time responses. The V2C3 configuration has the largest eddy current, which is in agreement with the

hypothesis that the Sol coil plays the dominant role on the creation of eddy currents, since in the V2C3 set-up, the Sol coil current is increased while the PF and Div coils currents are decreased. In order to get a deeper understanding of the eddy currents in the vessel, the highest eddy currents in each vessel's filament have been found, and plotted in Figure 5.6. The highest eddy currents of the different filaments do not correspond to the same time. It can be seen that the highest values of the highest eddy currents are induced near the coils with high currents, so that the inner side of the vessel displays the highest eddy currents, since it is the closer side to the Sol coil. Also the top and the bottom of the vessel display high eddy currents because of the Div coils. The V1C1, V2C2 and V2C3 set-ups displays the same A · turn on their coilset, but the V1C1 set-up displays lower eddy currents on the top and the bottom of the vessel. This difference must be caused by the shape of the vessel, so a D-shaped vessel is a better option in order to reduce the eddy currents. V2C3 displays similar values of the eddy currents to the V1C1 configuration, despite of the difference in the A · turn of their coilsets.

Using the eddy currents of figure 5.6, the magnetic forces the vessel has to withstand have been calculated. With the forces, the stresses on the vessel have been calculated in the limit of infinitely thin wall[3]. They are shown in figure 5.7. Table 5.3 shows the highest value of the radial and axial stresses. There is no toroidal stress since there is no toroidal component of the force, provided that the eddy currents flow in the toroidal direction. From the comparison between the V1C1, V2C1 and V2C2 set-ups, which have the same currents, it can be seen that the lowest radial stress correspond to the V2C1 set-up, while the lowest vertical stress correspond to the V1C1. Considering both values, the V1C1 set-up has to whithstand lower stresses, which also suggest that a D-shaped vessel could be the best shape. Moreover, as with the eddy currents, the V2C3 set-up displays lower stresses than the V1C1 set-up.

[3]The stress tensor is just a generalization of the pressure, an scalar magnitude. Pressure is the force per unit area if the force is perpendicular to the surface. If the force is not perpendicular to the surface, the stress tensor needs to be introduced. Since the magnetic force is a vector magnitude, the stress will also be a vector magnitude.

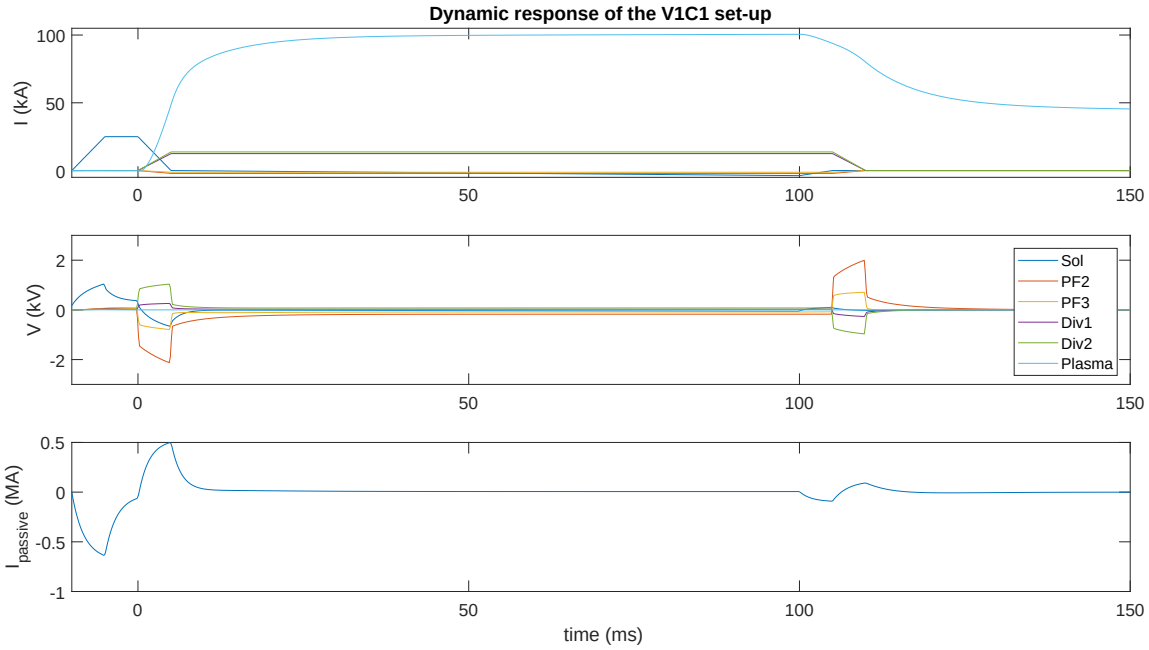

(a) V1C1.

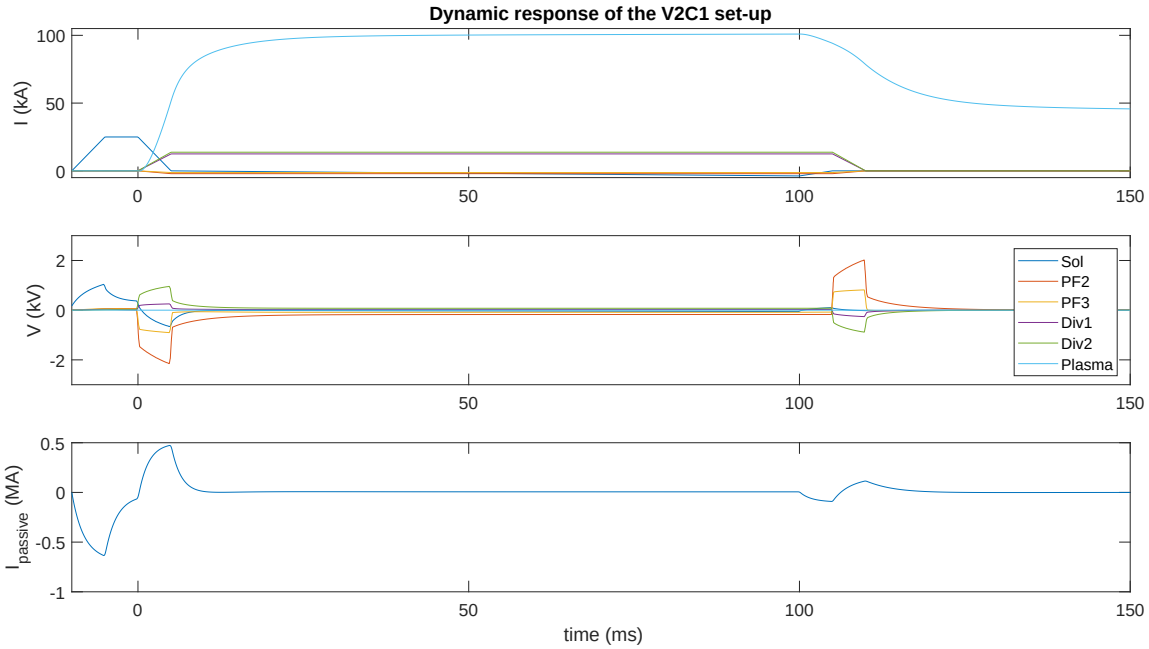

(b) V2C1.

Figure 5.4. Dynamic, or time response for the V1C1 and V2C1 set-ups. From top to bottom: the plasma and coilset currents (in kA, in figure 5.3 it is shown in MA · turn), their voltage and the total eddy current in the vessel, I_{passive}, as a function of time. It can be seen that in $t = 0$ the plasma currrent rises up to 100kA. It is maintained during 100ms with the same current, and after that the coilset is turned off. The plasma current decreases to half of its initial value, and then it slowly decreases. It has not been possible to ramp the plasma current down to zero, so others method of terminating the plasma discharge needs to be studied.

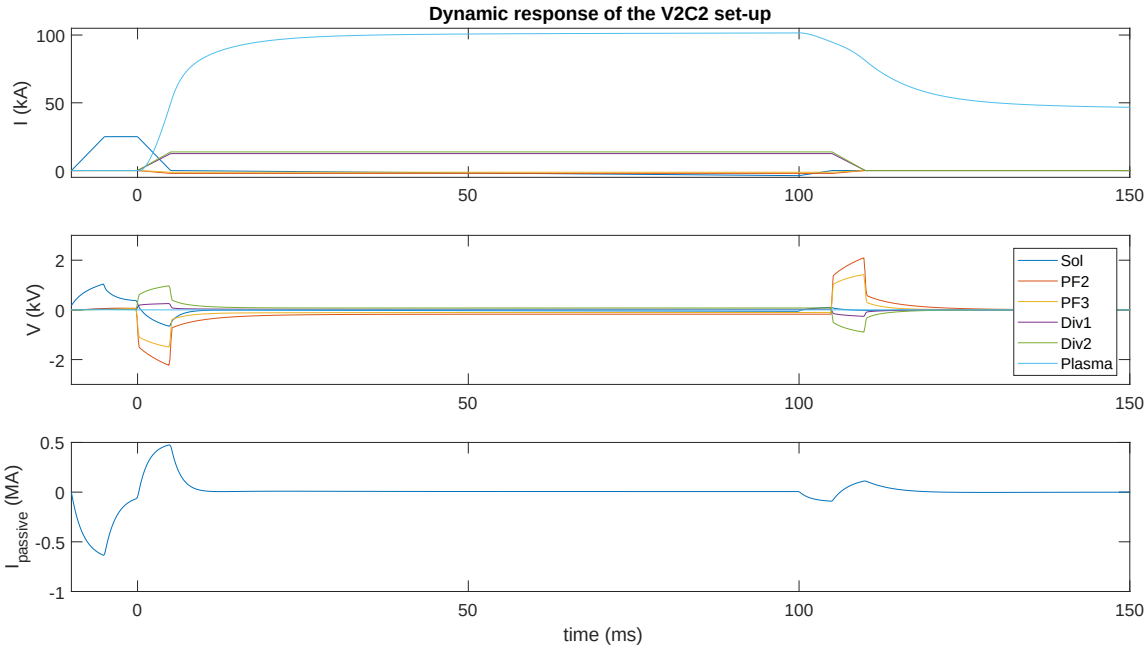

(a) V2C2.

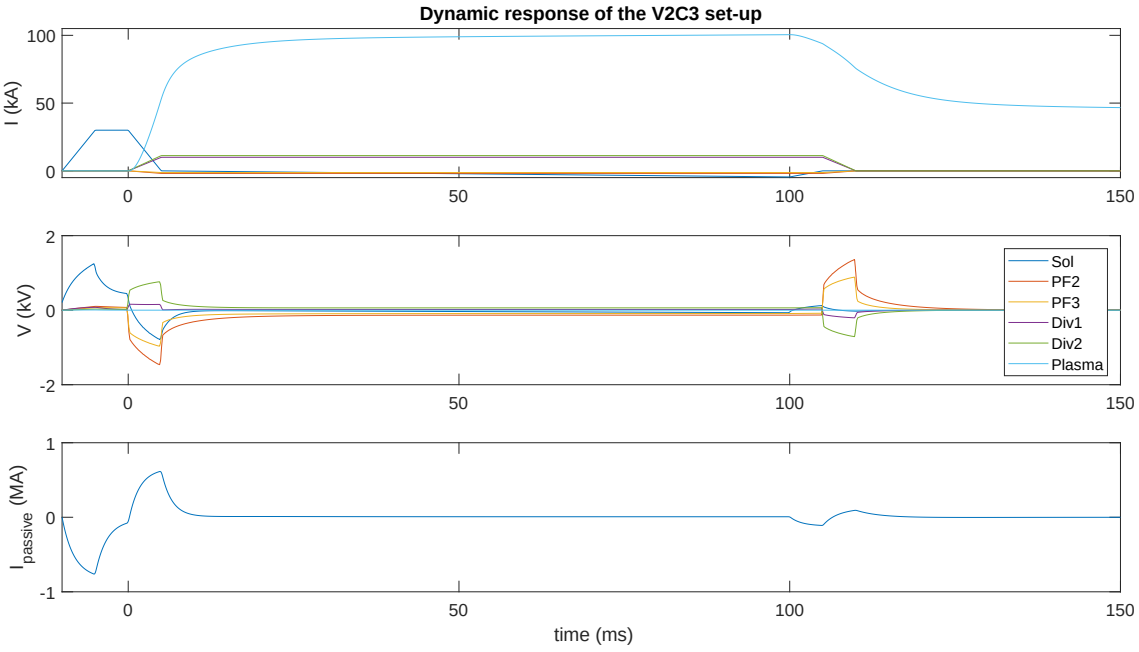

(b) V2C3.

Figure 5.5. Dynamic, or time response for the V2C2 and V2C3 set-ups. From top to bottom: the plasma and coilset currents (in kA, in figure 5.3 it is shown in MA · turn), their voltage and the total eddy current in the vessel, I_{passive}, as a function of time. It can be seen that in $t = 0$ the plasma currrent rises up to 100kA. It is maintained during 100ms with the same current, and after that the coilset is turned off. The plasma current decreases to half of its initial value, and then it slowly decreases. It has not been possible to ramp the plasma current down to zero, so others method of terminating the plasma discharge needs to be studied.

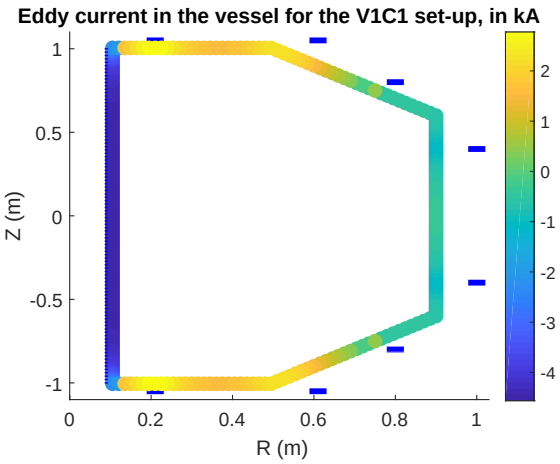

(a) V1C1.

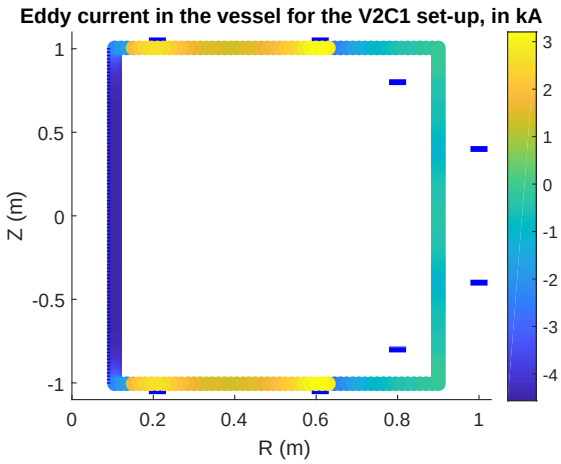

(b) V2C1.

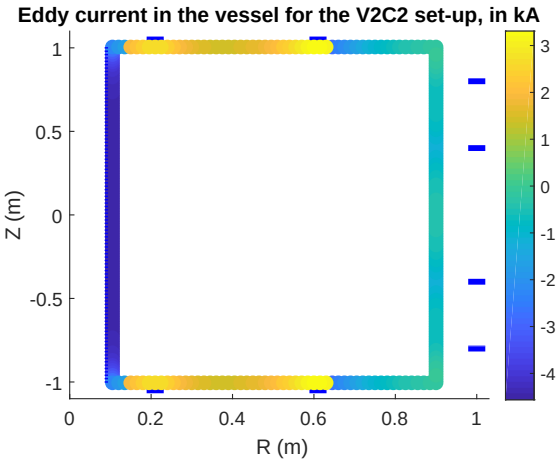

(c) V2C2.

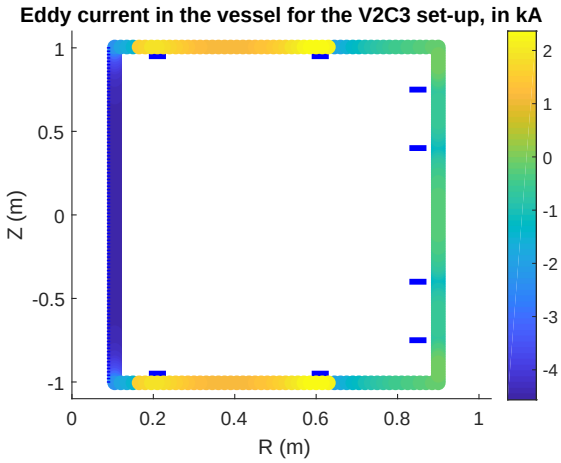

(d) V2C3.

Figure 5.6. Highest eddy currents induced in each vessel's filament, showed with a colourbar. The highest value of each filament do not correspond to the same time instant. The coilset is also shown.

Highest stresses on the vessel		
	Radial (kPa)	Vertical (kPa)
V1C1	39.015	31.550
V2C1	30.567	50.795
V2C2	30.837	51.672
V2C3	37.657	21.512

Table 5.3. Highest values of the radial and axial stresses acting upon the vessel for all the set-ups, in the limit of infinitely thin wall.

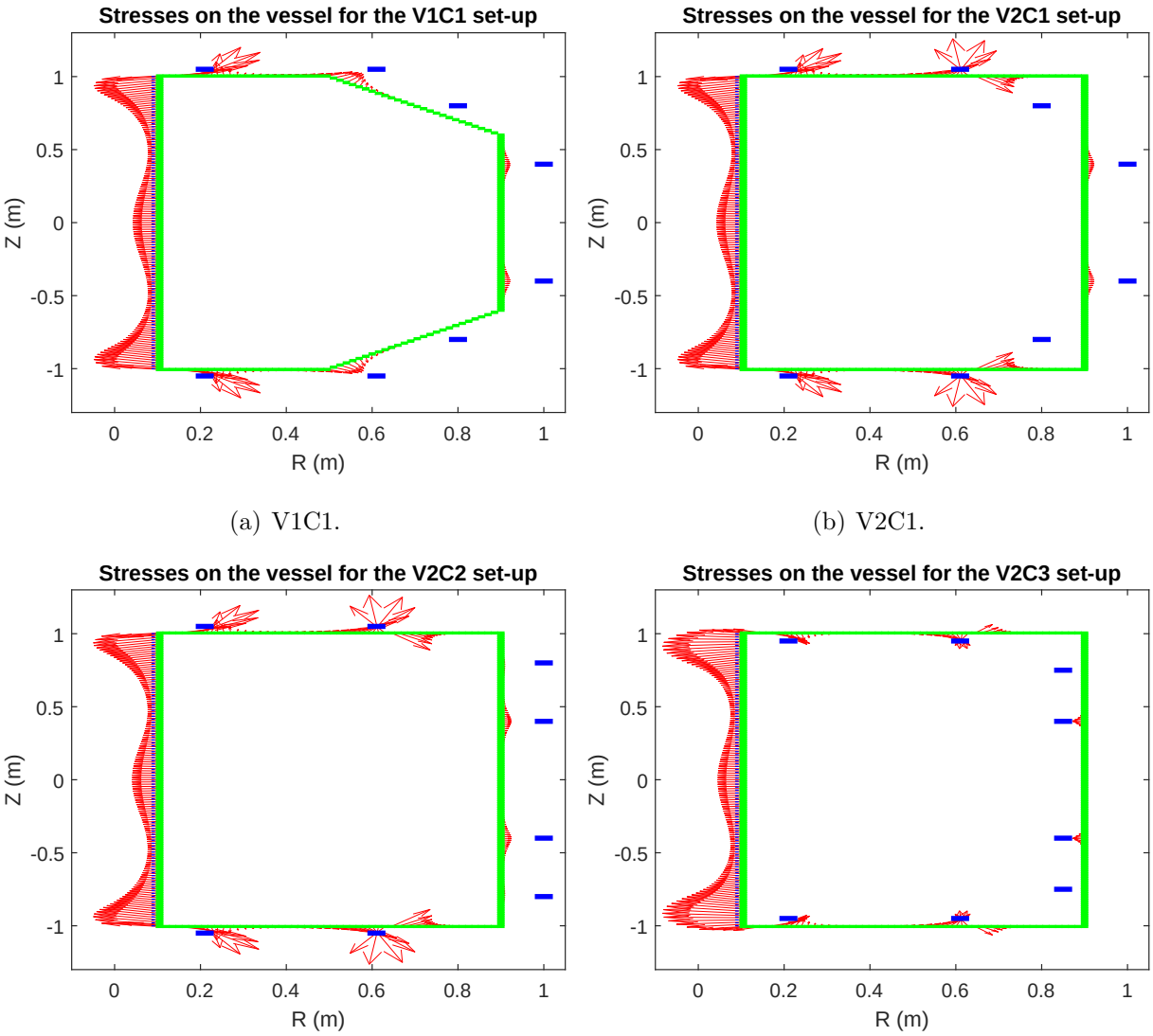

(a) V1C1.

(b) V2C1.

(c) V2C2.

(d) V2C3.

Figure 5.7. Highest stresses on the vessel for the differents set-ups, in the limit of infinitely thin wall. The stress is shown with red arrows, indicating its direction (the stress is a vector magnitude since the force is a vector magnitude). The vessel and the coilset are also shown. The arrows has a common scale so all the graph displays the same scale. In order to compare then, it is also needed to see table 5.3.

5.1 Discussion

It is mandatory to compare the results with the bibliography to assure the reliabilty of the results obtained, though this comparison have to be done carefully, since every spherical tokamak (ST) has its own coilset, geometry, etc. To do so, it have been taken into account severals ST of similar characteristics.

The first topic to discuss is the coil currrents. In [15], the first discharge of VEST is described, achieving I_p=60kA. VEST has its coilset outside the vessel[4]. Its PF9, PF10 coils could be compared with PF2 and PF3 coils of Seville ST due to their similar positions and role. Their current can reach -24 kA · turn, which is comparable to -50 and -30 kA · turn, the maximum currents used for PF2 and PF3 coils respectively. VEST has two inductor solenoids, used for the plasma start-up. The PF1 solenoid sustains the plasma, and it carries 1.9MA · turn, a lower current than the current the inductor solenoid in the simulations carry. This difference could be explained by considering its start-up, the VEST start-up relies on the creation of two small plasmas in the upper and lower chamber, that will be merged to the central chamber[5]. A discharge of the Globus-M2 ST is shown in [17]. It achieves I_p=500 kA. Its coilset is located outside the vessel. Their PF1 and PF2, which are divertor coils, carries a maximum value of 282 kA · turn , and its PF coil carries a maximum value of -140 kA · turn. These currents are higher than the currrents used in the simulations. Its inductor solenoid carries 4.4MA · turn, a higher current than the current used in this work for the inductor solenoid, 2.5 and 3.0 MA · turn. The fact that Globus-M2 currents are higher than the currents used in the simualtions could be understood by noting that Globus-M2 achieves a higher plasma current. By taking into account this two ST, it can be seen that the coilset current values used in this thesis are of the same magnitude order than the ones used on the cited tokamaks. However, it have to be noticed that their equilibria are different from the equilibria achieved here. Their plasma is very close to the inner wall of the vessel, and is big enough to fill most of the vessel's inner space, while the equilibria obtained here is smaller. The reason to choose the equilibrium used in this thesis is to optimise the elongation and the safety factor in order to enlarge the fusion power and particle confinement; bigger plasmas leads to

[4] See appendix B, where its cross-section, as well as the cross-section of the other ST used to compare with are shown.

[5] See [16] for further details.

greater triangularity and lower elongation, which means lower fusion power (see section 2.3), and also higher safety factor, that means low confinement (see section 2.3.2).

The eddy currents are strongly dependent on the wall thickness. Thinner walls means lower eddy currents (as an example, a wall width 0.08m leads to a highest eddy current of $\sim$ 140kA, leading to higher pressures on the vessel). But thinner walls are more computationally expensive, so the value choosen for the simulation tries to balance both the computational time and the need for a thiner vessel to reduce eddy currents. The time evolution of the eddy current in the vessel of the Globus-M ST is shown in [18]. Globus-M is a ST whose plasma current can achieve 360kA. The total eddy current reachs a maximum value of 50 kA, having its vessel a maximum thickness of 0.014m. The time evolution of the eddy current is shown in figures 5.4 and 5.5, and it can be seen that the eddy current can reach $\sim$ 4 kA, with a wall width of 0.015m. The distribution of the eddy current in the Globus-M vessel is described in [19]. Its maximum value is 7kA, while the maximun value achieved in the simulations carried out in this thesis is 4kA. From this, it can be noticed that the simulations carried out here displays lower eddy currents. The greater eddy currents of Globus-M could also be understood by considering its plasma current, which is greater than the plasma current achieved in the simulations carried out.

The normal stress the Globus-M vessel has to withstand is also included in [19]. Its highest value is 17kPa, while the highest value obtained in the simulations carrieed out is 40kPa, a larger value, but with the same magnitude order. The value obtained, as said previously, could be reduced by decreasing the vessel's wall width.

It has to be reminded that this is the first approach to the search for an equilibrium for the Seville ST, exploring for the first time four different set-ups, while the ST used to compare with are now-operating tokamaks, highly optimized. Nevertheless, the results of the simulations, as discussed above, are similar to the parameters of now operating ST, which could confirm the reliability of the simulations carried out.

On the other hand, several parameters such as the number of turns, the width and heihgt of the coils, or the plasma resistance have not been modified, but their effect may play an important role on the search of the final set-up for the Seville ST. The main role of the plasma resistance is to enlarge or reduce the plasma discharge, i.e., to increase or reduce the decreasing rate of the plasma current, such that high values of the resistivity mean faster decreasing of the plasma current. The coil temperature does not play an

important role on the simulations, as it has been tested that coil temperatures variations leads to no changes. Changes in both the coil's width and heigh results in a change of the equilibrium configuration, and as a consequence a change in the stresses and eddy currents, since it affects the distance between the vessel and the coilset. Changes in the number of turns are irrelevant as long as the product A · turn remains constant. If it does not remain constant, the equilibrium will be modified, so the eddy and the pressures also will be modified. The ramp up and down rates of the coilset have been arbitrarily set. Changing them affects the eddy currents, faster rates means higher eddy currents, which also means higher pressures.

So far, four different configurations for the future Seville ST have been explored. A comparison between the set-ups is included.

- V1C1 vs V2C1 (vessel's shape)

  V1C1 has, with respect to V2C1:

  - Same currents
  - Lower κ and $q95$, greater β (all of them)
  - Lower eddy currents and stresses

- V2C1 vs V2C2

  V2C1 has, with respect to V2C1:

  - Same current
  - Lower κ and β, and higher $q95$
  - Similar eddy currents
  - Lower stresses

- V2C2 vs V2C3

  V2C2 has, with respect to V2C3:

  - Lower coilset current
  - higher κ, $q95$ and β_{p}, lowest β_{T} and β_{N}
  - higher eddy currents
  - higher stresses

From the comparison between the V1C1 and the V2C2 set-ups it is concluded that the best shape of the vessel is D-shaped, since the difference in the κ is negligible. The comparison between the V2C1 and the V2C2 set-ups is not as straightforward as the previous, since the V2C2 set-up has better equilibrium parameters with the exception of κ, but it has to stand hihger pressures. The comparison between V2C2 and V2C3 is not trivial too, but taking into account the increase in the coilset current, V2C2 could be a better option.

Chapter 6

Conclusions

In this thesis an exploratory analisis of four different configurations of the future Seville spherical tokamak has been carried out, testing different coilset configuration and vessel's shape. The fundamental concepts about tokamaks and toroidal magnetic fusion devices have been introduced, as well as the fundamental physics underlying tokamaks. The study have been done using the FIESTA code, an object oriented code programmed in MATLAB. A similar equilibria has been achieved for all the configuration, and a comparison between the current needed to achieve that equilibria in the different set, as well as the eddy currents induced in the vessel and the stresses the vessel has to withstand have been done.

The optimum vessel's shape have been found to be D-shaped, but the results for the coilset configuration have not been conclusive. This is due to the fact that the equilibrium parameters to determine the best coisel configuration more research needs to be done since the study have not been done with the optimised shape, and ifs effect may be determinant to choose the best configuration. Several parameter, which may play an important role on the search on the optimal coilset configuration have not been included in the study. These parameters are fundamentally the coilset size. Also an study about the termination of the tokamak's discharge needs to be done. However, this will not modify the results obtained here such as the maximum eddy currents or the stresses since the highest stresses and eddy currents appear at the begining of the discharge due to the inductor solenoid. Also, the ramp up and down rates of the coilset have been arbitrarily set, and may not correspond to the component used in the construction. These rates are fundamental parameters for the eddy current, and therefore for the stresses.

Bibliography

[1] J.Wesson *Tokamaks*. 4^{th} edition. Oxford University Press, 2004.

[2] Francis F. Chen. *Introduction to Plasma Physics and Controlled Fusion*. 3^{rd} edition. Springer International Publishing, 2016.

[3] A. Pironti et al. "Fusion, tokamaks, and plasma control". *IEEE Control Syst. Mag.*,vol *25*, no. *5*, pp. 30–43, Oct 2005.

[4] A. Beghi et al. "Advances in real-time plasma boundary reconstruction". *IEEE Control Syst. Mag.*,vol *25*, no. *5*, pp. 44–64, Oct 2005.

[5] M. Ariola et al. "Plasma shape control for the JET tokamak". *IEEE Control Syst. Mag.*,vol *25*, no. *5*, pp. 65–75, Oct 2005.

[6] G. Ambrosino et al. "Magnetic control of plasma current, position, and shape in tokamaks". *IEEE Control Syst. Mag.*, vol *25*, no. *5*, pp. 76-92, Oct 2005.

[7] YuhongXu. "A general comparison between tokamak and stellarator plasmas". *Matter and Radiation at Extremes*,vol *1*, issue *4*, pp. 192-200, July 2016.

[8] Y-K. M. Peng et al. "Features of spherical torus plasmas". *Nuclear fusion*, vol *26*, p. *769*, 1986.

[9] Jeffrey P. Freidberg *Ideal Magnetohydrodynamics*. 1^{th} edition. Plenum Press (New York and London), 1987.

[10] T.C. Luce. "An analytic functional form for characterization and generation of axisymmetric plasma boundaries". *Plasma physics and Controlled fusion*,vol *55*, no. *9*, July 2013.

[11] Stanley M. Kaye et al. "Physics design of the national spherical torus experiment". *Fusion science and technology*, vol. *36*, issue *1*, July 1999.

[12] J.B. Lister et al. "Plasma equilibrium response modelling and validation on JT-60U". *Nuclear Fusion*, vol *42*, no. *6*, p. 708, June 2002.

[13] A. Coutlis et al. "Measurements of the open loop plasma equilibrium response in TCV". *Nuclear Fusion*, vol *39*, number *5*, 1999.

[14] M.G. Sevillano-Berasategui et al. "Review of Tokamak Codes". Published at the 5^{th} International Conference on Electrical Engineering, Computing Science and Automatic Control, 2008.

[15] YoungHwa An et al. "Plasma start-up and first plasma experiment in VEST". *Fusion engineering and design*, vol *96-97*, pp. *274-280*, October 2015.

[16] K. J. Chung et al. "Design Features and Commissioning of the Versatile Experiment Spherical Torus (VEST) at Seoul National University". *Plasma Science and Technology*, number *15*, page *244*, 2013.

[17] V.B. Minaev et al. "Magnetic system for the upgraded spherical tokamak Globus-M2". *IAEA*, vol *5*, Report IAEA-CN–197, 2012.

[18] V. Amoskov et al. "Simulation and analysis of eddy currents induced in the GLOBUS-M tokamak". *Plasma devices and operations*, vol *13*, issue *1*, 2005.

[19] N. V. Sakharov et al. "Characterization of mlasma major disruption in the Globus-M spherical tokamak". *Plasma physics report*,vol *43*, issue *2*, pp. 422-432, April 2017.

[20] Norman S. Nise. *Control System Engineering*. 7^{th} edition. John Wiley & Sons, 2015.

Appendix A

State Space representation

The State Space representation[1] is a mathematical model of a physical system, which is shown in figure A.1. The system can be represented by the following system of equations:

$$\begin{cases} \dfrac{d\boldsymbol{x}}{dt} = \boldsymbol{A}\boldsymbol{x} + \boldsymbol{B}\boldsymbol{u}, \\ \boldsymbol{y} = \boldsymbol{C}\boldsymbol{x} + \boldsymbol{D}\boldsymbol{u}, \end{cases} \tag{A.1}$$

The column vector $\boldsymbol{x}$ contains the state space variables (the minimun set of variables needed to determine the system), and it is called the *state vector*. $\boldsymbol{u}$ is the *input or control vector*, which contains the input variables, and $\boldsymbol{y}$ is the *output vector*, and contains the output variables. $\boldsymbol{A}$ is the *system matrix*, and defines the first-order differential equations that determines the state variables, $\boldsymbol{B}$ is the *input matrix*, which relates the input variables with the time derivatives of the state variables. $\boldsymbol{C}$ is the *output matrix*, which defines the set of equations that determines the output variables as a combination of the state space variables and the inputs, and $\boldsymbol{D}$ is the *feedforward matrix*, which relates the input and output variables.

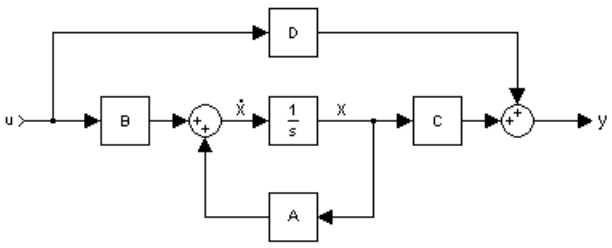

Figure A.1. Block diagram representation of the linear state-space equations. Source: https://en.wikipedia.org/wiki/State-space_representation.

[1] See [20], section 3.3, for a detailed description.

Appendix B

Cross-sections of the ST used to compared with the Seville ST

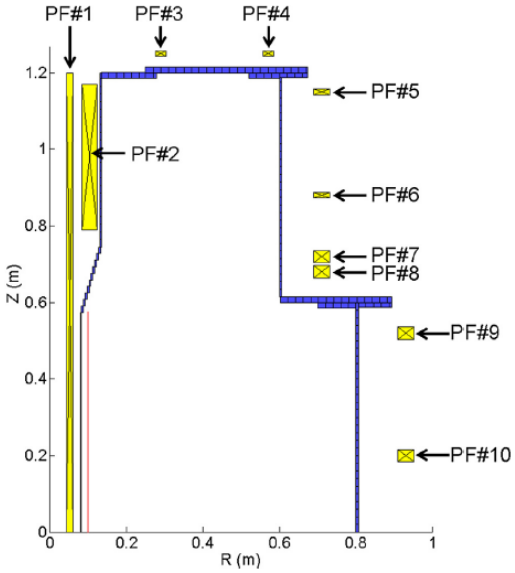

(a) Cross-section of the VEST ST. Source: [15].

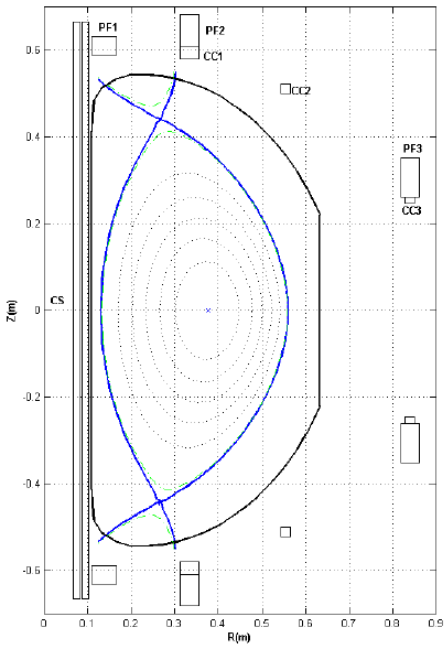

(b) Cross-section of the Globus-M2 ST. GLobus-M displays a very similar cross-section. Source: [17].

Figure B.1. Cross-section of the ST used to compared with the Seville ST.